

Draft

# The Phoenix Deep Survey: Optical and near infrared imaging catalogs

M. Sullivan<sup>1,2</sup>, A.M. Hopkins<sup>3,9</sup>, J. Alonso<sup>4</sup>, A. Georgakakis<sup>5</sup>, B. Chan<sup>6</sup>, L.E. Cram<sup>7</sup>, B. Mobasher<sup>8</sup>, C. Elmehdai<sup>4</sup>

1. Department of Physics, University of Durham, South Road, Durham, DH1 3LE, UK
2. Department of Astronomy and Astrophysics, University of Toronto, 60 St. George Street, Toronto, ON M5S 3H8, Canada
3. Department of Physics and Astronomy, University of Pittsburgh, 3941 O'Hara St, Pittsburgh, PA 15206, USA
4. CAAUL, Observatorio Astronómico de Lisboa, Tapada da Ajuda, 1349-018 Lisboa, Portugal
5. Institute of Astronomy and Astrophysics, National Observatory of Athens, I. Metaxa & B. Pavlou, Penteli, 15236, Athens, Greece
6. School of Physics, University of Sydney, NSW 2006, Australia
7. Australian Research Council, GPO Box 2702, Canberra ACT 2601, Australia
8. Space Telescope Science Institute, 3700 San Martin Drive, Baltimore, MD 21218, USA
9. Hubble Fellow

sullivan@astro.utoronto.ca

## ABSTRACT

The Phoenix Deep Survey is a multi-wavelength galaxy survey based on deep 1.4 GHz radio imaging (Hopkins et al., 2003). The primary goal of this survey is to investigate the properties of star formation in galaxies and to trace the evolution in those properties to a redshift  $z = 1$ , covering a significant fraction of the age of the Universe. By compiling a sample of star-forming galaxies based on selection at radio wavelengths we eliminate possible biases due to dust obscuration, a significant issue when selecting objects at optical and ultraviolet

wavelengths. In this paper, we present the catalogs and results of deep optical (UBVRI) and near-infrared (Ks) imaging of the deepest region of the existing decremental radio imaging. The observations and data-processing are summarized and the construction of the optical source catalogs described, together with the details of the identification of candidate optical counterparts to the radio catalogs. Based on our UBVRIKs imaging, photometric redshift estimates for the optical counterparts to the radio detections are explored.

**Subject headings:** surveys { cosmology: observations { radio continuum : galaxies { galaxies: photometry { galaxies: evolution { galaxies: starburst

## 1. Introduction

The study of galaxy evolution in recent years has included a strong focus on the star formation properties of galaxies (Lilly et al. 1996; Maddalena et al. 1996; Connolly et al. 1997; Adelberger & Steidel 2000; Haarsma et al. 2000; Sullivan et al. 2000; Hopkins et al. 2000b; Buat et al. 2002; Condon et al. 2002; Tresse et al. 2002; Gomez et al. 2003). Many of these studies draw their galaxy samples primarily from selection at ultraviolet (UV) or optical wavelengths (for example broad-band imaging or through the H $\alpha$  emission line), and are known to be affected by obscuration due to dust intrinsic to the galaxies of interest. Correcting for the effects of this dust has been shown to be a complex problem, especially for distant objects (e.g. Calzetti 2001); furthermore selection at optical and UV wavelengths results in samples of star forming systems which may omit a significant fraction of heavily obscured galaxies (Smail et al. 2002). A related issue is that the most strongly star-forming systems are on average the most heavily obscured (Hopkins et al. 2001; Sullivan et al. 2001; Buat et al. 2002; Hopkins et al. 2003c; Afonso et al. 2003), with recent results suggesting an average Balmer-decrement derived obscuration of radio-detected systems of  $A_H \sim 1.6$  (Afonso et al. 2003; Hopkins et al. 2003c), higher than in UV or H $\alpha$  selected samples ( $A_H \sim 1$ ; Tresse & Maddox 1998; Sullivan et al. 2000).

Selecting galaxies at radio or far-infrared (IR) wavelengths could alleviate many of the potential problems associated with selecting galaxies at optical/UV wavelengths. Far-IR emission is a by-product of massive star formation, a result of UV radiation being absorbed by dust and re-emitted in the 10–300 m wavelength range. The existence of a tight and linear relationship between this far-IR emission and radio luminosity in local galaxies (e.g., de Jong et al. 1985; Condon et al. 1991; Bell 2003) suggests a strong link between radio emission and unobscured massive star formation, though the specific details of the physical model of the radio emission are still poorly understood theoretically (Condon 1992). Hence,

selecting at radio wavelengths can provide samples of star-forming galaxies without regard to their intrinsic dust content.

In order to identify a homogeneously selected catalog of star-forming galaxies, unbiased by obscuration-based selection effects, and spanning a broad redshift range ( $0 < z < 1$ ), the Phoenix Deep Survey (PDS<sup>1</sup>) relies on a deep 1.4 GHz mosaic image, based on observations with the Australia Telescope Compact Array. This has been used to construct one of the largest existing deep 1.4 GHz source catalogs (Hopkins et al. 2003a) from which a star-forming galaxy sub-sample can be drawn. The PDS has already been highly successful in providing a basis for several investigations of the nature of star-forming galaxies and their evolution (e.g., Georgakakis et al. 1999a,b; Mobasher et al. 1999; Hopkins et al. 2000a; Georgakakis et al. 2000; Afonso et al. 2003). Additionally, 2dF spectroscopic information exists for a large fraction of the optically brighter optical counterparts (Georgakakis et al. 1999a).

In this paper, we present the details of deep optical and near-infrared (NIR) imaging carried out over the deepest portion of the 1.4 GHz radio survey. These observations will, in later papers, be used to investigate the star formation and dust properties of the faint radio source population, and the evolution of these properties out to  $z' \approx 1$ . A plan of this present paper follows. In Section 2, we present the various imaging datasets and discuss the steps taken to reduce the raw data. Section 3 describes the processes involved in creating robust source catalogs drawn from the optical imaging, and the technique used to cross-correlate this optical dataset with the existing radio catalog. In Section 4 we investigate the degree to which photometric redshift estimates can be made for our radio-selected sample, and in Section 5, we discuss the broad photometric properties of the radio-selected sample. We summarize our results in Section 6. Throughout this paper we assume  $\Omega = 0.7$ ,  $M = 0.3$ ,  $h = 0.70$  (where  $H_0 = 100 h \text{ km s}^{-1} \text{ Mpc}^{-1}$ ) cosmology.

## 2. Imaging datasets

In this section, we describe the imaging observations of the PDS. This comprises three primary sets: AAT wide-field imager (WFI) optical BVRi data, CTIO MOSAIC-II U-band data, and ESO-WFI U-band data. These imaging cameras cover approximately the same area on the sky (around  $0.35 \text{ deg}^2$ ) and hence the same mosaicing pattern was used at each telescope to facilitate the alignment of data from different filters. The extent of the coverage of the radio field and the numbering of the pointing pattern used in relation to the deep radio survey can be seen in Figure 1. In addition to the optical data, near-IR NTT/SO fit

---

<sup>1</sup> see also <http://www.atnf.csiro.au/people/ahopkins/phoenix/>

K s data also exists for part of the central pointing (see pointing 7 in Figure 1), as well as relatively shallow AAT R and V-band data ( $m_R' \approx 22.5$ ) from most of the PDS fields presented in Georgakakis et al. (1999a). Below we describe the observations and reduction of the new optical datasets; the observations in this section are summarized in Table 1.

### 2.1. Optical imaging observations

The following observations were taken. Two pointings (7,3) were observed in BVR*i* and one (pointing 11) in BVI on the nights of August 13 and 14 2001, with the WFI camera on the AAT. The same three pointings were also observed in U with the MOSAIC-II camera on the CTIO 4m Blanco telescope on September 3rd 2002. Finally, four of the PDS fields (2,3,6,7) were observed in U with the WFI on the ESO 2.2m on the night of August 18 2001. All exposure sequences were dithered to cover the inter-chip spacing; details can be found in Table 1. All the science observations were interspersed with observations of standard star fields taken from Landolt (1992) { all the data presented in this paper were secured during photometric nights.

We will not discuss the reduction of the individual datasets, as these typically followed the same path; instead we outline the generic reduction steps below and discuss issues specific to each dataset reduction where appropriate. All the data were reduced using iraf and the National Optical Astronomy Observatories (NOAO) MOSAIC reduction software package mscred version 4.7 (Valdes 1998), as well as some custom-written routines where required. Data were bias-subtracted using overscan regions and a master bias frame generated on each night of observation. Flat-fielding was performed using dome-ats (BVR*i* data) in the standard manner. For U-band data, dome-ats provide a poor flat-field correction and consequently we flat-field these data using twilight sky-ats. Bad-pixel masks are also generated for each image, containing bad column, saturated stars, and bleed trails identified by mscred.

Astrometric solutions were applied to each science frame using the iraf TINY projection. For CTIO U-band data we applied the distortion correction provided by the observatory. For the AAT and ESO data we generated our own distortion corrections from the observation fields and USNO-2 stars. These solutions were typically accurate to  $\sim 0.35''$ . The astrometrically calibrated frames were then projected and re-sampled using a sinc function onto a standard linear world coordinate system (WCS) with a constant pixel-scale, linearly interpolating over bad-pixels to avoid ringing effects in the re-sampled data. The re-sampling was performed so that each image for a particular pointing was placed onto the same pixel coordinate system { in general we aligned to the CTIO MOSAIC-II system which has the

largest field-of-view and the most precise WCS. The realignment process is accurate to 0.1''. In order to combine data in each filter, we determined the sky levels in each image as follows. We ran sextractor (Bertin & Arnouts 1996), outputting a FITS file object mask. We then used an iterative technique to determine the modal pixel value, excluding those pixels lying within object boundaries determined by the sextractor mask. The modal value was subtracted from each data frame, and the rms dispersion in the sky level recorded.

The individual dither steps at each pointing were then median-combined, masking cosmic-rays, chip defects and satellite trails, creating the deepest possible final image for each pointing. We applied multiplicative scaling factors to each image (calculated from common USNO-2 stars) to allow for airmass variations between exposures – zero-point offsets were not required due to the previous subtraction of the modal sky value. The result is an astrometrically-calibrated and photometrically-stable combined science image. Finally, the modal sky value was added back to preserve the count statistics for later analyses.

The photometric calibration was performed using stars drawn from the catalog of Landolt (1992). These frames were observed at a variety of airmasses throughout the night, with an effort made to ensure that standard stars fell on each chip in the mosaic arrays. Zeropoints were derived from these data in the standard way, and the large number of stars observed allowed us to fit for both the zeropoint and airmass/color terms. We found negligible color terms (less than 0.02 mag) in the BVR data relative to the standard Johnson-Cousins system (e.g. Bessell 1990), suggesting these filters/CCD response systems approximate well to the standard calibration system. As the i-band data, however, were obtained through an SDSS i-band filter and not a Cousins-I filter ( $I$ ), a non-negligible color term was required to align these data into the  $I_c$  system of the standard stars. We found that to convert our measured CCD photometry with this filter,  $i_{\text{CCD}}$ , to the standard Cousins system ( $I_c$ ) required a transformation of the form

$$I_c = i_{\text{CCD}} - 0.194(R_c - I_c); \quad (1)$$

where  $i_{\text{CCD}}$  is the calibrated i-band magnitude with no color term applied, and  $R_c$  is the calibrated R<sub>c</sub>-band magnitude.

The U-band data also possess small color terms, though this is harder to calculate due to the limited precision to which Landolt (1992) stars have been observed in the U. Indeed, a large uncertainty connected with U-band imaging is the accuracy, and consistency, to which a photometric calibration can be performed, due to the high sensitivity to even small amounts of cirrus, and the effect of varying site-to-site extinction laws.

We are fortunate, however, to be able to perform an internal test on the consistency of

our U-band data. As two of the ESO pointings overlap with the CTIO U-band data (numbers 3 and 7), we can test the precision of our U-band photometric calibration by comparing the aperture magnitudes of objects common to both datasets. In the coinciding frames we measure 3<sup>0</sup>-diameter aperture magnitudes for the objects detected by sextractor, the comparison of which is shown in Figure 2. The agreement between the two datasets is excellent; the median offset is 0.01 mag for ESO detections with  $U < 21$ , and -0.03 mag for all objects which lie above the limiting magnitude of the ESO data. Given that these data were taken at different sites with different telescope/instrument combinations, this represents a highly encouraging consistency check between our U-band datasets. Where common objects are observed between the two datasets, we always take the CTIO magnitudes as our default measure due to the greater depth of these data.

## 2.2. Near infrared NTT/SO observations

Our NIR imaging data come from the Hawaii HgCdTe 1024x1024 pixel-array SoFI camera on the 3.6m ESO New Technology Telescope (NTT). The field-of-view was 4.9°x4.9° with a pixel scale of 0.29". Nine contiguous pointings, in a 3x3 pattern, were observed over the deepest region of the PDS (a sub-region of pointing 7; see Figure 1), during October 10 and October 11 2000. At each pointing, 45 dithered 60s exposures were taken in the Ks filter, except for the central pointing where this sequence was repeated 4 times. Each 60s exposure comprised the average of six 10s sub-exposures. All data were taken under photometric conditions with seeing of less than 1.2".

The raw data were reduced using iraf following a method developed by Peter Whitmore and Will Saunders, outlined here. To correct for the varying pixel responses to light from astronomical objects, an image of a source with uniform light intensity over the entire field-of-view is required. Ideally we require two such images. The first is a standard NIR dome flat, appropriate for correcting the pixel-to-pixel variations in response to astronomical objects. This is created by averaging the subtraction of many "dome-light-on minus dome-light-off" image pairs. However, this dome flat is not appropriate for correcting for the response to variable sky illumination. It is the highly variable nature of this NIR night-sky that makes this second flat important, as we mustatten the pixel response to the night-sky before subtracting the sky background. The method we use here makes use of a technique which uses the night-sky itself as this second flat.

The procedure is as follows. First, all the raw science frames were median combined to produce a super-sky image, which was then subtracted from every raw data frame. The differences between consecutive "supersky-subtracted" science frames was then calculated,

giving the spatial and temporal changes in sky brightness levels from frame to frame. As these differences from frames are noise dominated due to the small amplitude of the sky fluctuations, they are normalized and combined to make a high-S/N template. This "difference-template" is then divided into all the science frames, correcting for the variable pixel response to the sky illumination.

To subtract the remaining sky level in each individual science frame, the 8 temporally closest science frames are median-combined (masking stars and bright objects) and the result subtracted from that science frame, leaving a sky-subtracted image. Multiplication by the difference-template and then division by the template then corrects for the varying pixel-to-pixel response to light from astronomical objects.

The photometric calibration was performed using infrared standards from Persson et al. (1998), observed throughout each night. We also dithered one standard star across the array as a check on the astrometry; the dispersion in the measured magnitudes of this standard star was 0.015 mag. The photometric calibration was similar for each night, and we derived a common solution with an rms scatter of 0.02 mag.

The sub-images were then registered and combined, first for each individual pointing, and then finally for the full 14 arcmin mosaic, masking chip defects. Astrometric calibration was made using the SUPERCOSMOS catalog, with 40 stars identified and used to build the astrometric solution. The rms of the solution was  $\sim 0\farcs2$ , similar to that found in the optical imaging. As a final step, the Ks mosaic was re-sampled to the same WCS and pixel scale as the optical data in pointing 7 for use in constructing the source catalogs.

### 2.3. Aligning the magnitude system

Each of our datasets have been calibrated to the standard Vega-based magnitude system using Landolt (1992) standard star fields. We prefer, however, to apply further corrections in order to place our magnitudes onto the easily-interpretable AB-magnitude system (e.g. Oke 1974), defined as

$$m_{AB} = -2.5 \log(F) - 48.60 \quad (2)$$

where the flux,  $F$ , is in units of  $\text{erg s}^{-1} \text{cm}^{-2} \text{Hz}^{-1}$ . This system allows an easy conversion into fluxes for any magnitude. Conversions for the B V R I Ks magnitudes were calculated using the standard filter responses. For the U-band data we use the filter responses as measured

for the system in use at the telescope. The AB conversions are listed in Table 2, and are similar to conversions tabulated in the literature (Fukugita et al. 1995).

### 3. Source detection and catalog construction

To make full use of our multi-wavelength dataset, we require robust and reliable catalogs drawn from each observation set, containing all objects present in all passbands. In this section, we describe the technique used to construct the source catalogs from our data.

#### 3.1. Preliminaries

Our principle tool in constructing the optical catalogs is sextractor version 2.2.2 (Bertin & Arnouts 1996), which we run from within custom-written perl routines which handle the various aspects of the catalog construction. We first determine the seeing in each data frame using a perl routine, running sextractor using a high detection threshold and an estimate of the seeing based on visual inspection using imexamne. From the catalog of detected, bright objects, we extract a list of objects classified as stellar according to the sextractor neural network classifier. We feed this list to the phot package in iraf, fitting Gaussian profiles to each object, rejecting all objects with fitted ellipticities of  $< 0.95$  as well as those which lie near to the edge of a particular image. The 100 objects with the smallest fitted FWHM are extracted, and the median FWHM value of this list taken as the seeing estimate for that image. In general, the seeing of all the images is very similar as conditions were stable during the observations. The exception is the K s-band data, which was taken in superior seeing conditions. The measured seeing values are listed in Table 3. Finally, we convolve each image to the poorest seeing of the observation set, and generate two catalogs, one containing seeing-matched data and the other the original data. Again, with the exception of the K s-band data, this step is not critical.

#### 3.2. Catalog completeness limits

For the final catalog construction, we also need to estimate the completeness magnitudes for each image. We estimate this in two ways. Firstly, we estimate the 5-limiting magnitude for each image. We use sextractor to detect a catalog of objects, sorting the list based on the errors in the object magnitudes. The 5-limiting magnitude is taken as the median magnitude of all objects with magnitude errors in the range 0.19–0.21, and the values are

listed in Table 3.

The other approach is to estimate 50 and 80% completeness limits by inserting fake sources into our imaging data, and measuring the fraction recovered as a function of magnitude. Our procedure is as follows. For each filter, we insert into the images sources at random (but recorded) positions with a magnitude distribution which follows the galaxy number counts of McCracken et al. (2003), the total number inserted normalized to the effective area of each pointing. Each source is inserted with a FWHM determined in Section 3.1. Using sextractor, we determine how many of these sources are recovered as a function of magnitude. This simulation is repeated 100 times for each pointing/filter combination, and the magnitude at which 50% and 80% of sources are recovered is recorded (see Figure 3 for example histograms of these distributions from the pointing PDF-7). The estimated completeness limits for each pointing and filter are listed in Table 4.

### 3.3. Constructing the detection image

With large mosaic images across up to six photometric bands, constructing reliable object catalogs, containing all possible detections from all available bands, is a complex task. For example, if we choose to detect objects in only one passband and then measure magnitudes in the remaining passbands using the positional parameters derived from the detection image, we will likely (1) exclude objects with unusual colors, and (2) miss detections that, while not significant in any one passband, are clear detections when all the available data is combined. As one of the goals of this project is to detect the very-faint optical counterparts to a deep radio survey, having a source catalog with all possible detections is clearly important. The alternative approach of matching catalogs created for each individual passband will solve the first problem (though not the second), but introduces complex uncertainties if different apertures are used for magnitude measures in different passbands.

We choose to use a modified version of the multicolor object detection technique of Szalay et al. (1999). Essentially, this is a  $\chi^2$ -technique. We construct a "detection" image from  $N$  different passbands by co-adding, for each pixel, the sky-subtracted flux ( $f$ )s weighted by the dispersion in the sky ( $s$ ) according to

$$\chi^2 = \sum_{i=1}^N \left( \frac{f_i}{s_i} \right)^2 \quad (3)$$

This technique is particularly suited to our dataset, as all the optical data were taken at the same position in the sky, and hence the pixels in the  $\chi^2$  image have contributions from

all the passbands.

This technique assumes that each image is sky-noise limited, and that the depth is constant across the mosaics. In practice this is not always true due to the dither pattern used to remove the inter-chip gaps in the CCD mosaic leading to some small regions with increased noise when compared to the mosaic as a whole; however, as each pointing is typically comprised of several individual exposures, the approximation to a constant noise level is good away from the edges of the images. We exclude the U-band data in constructing the detection image, as the B V R I K s images contain all the objects detected in U, and the addition of the U-band data typically degrades the quality of the  $^2$  detection image.

### 3.4. Photometric measurements

To construct the photometric catalogs, we run sextractor using the  $^2$  images as the detection images and measure from each of U B V R I K s images with the modal sky level added back, filtering using a Gaussian matched to the seeing FWHM. Objects are included in the  $^2$ -image-detected output catalogs if, in the  $^2$  image, they contain 4 or more contiguous pixels above a pixel detection threshold at which the distribution of "sky" and "object" pixels cross (see Szalay et al. 1999). This threshold is somewhat conservative, minimizing the number of false detections. Objects containing bad-pixels (e.g. saturated stars and bleed trails) in either the detections or measurement images are flagged in the output catalogs. We measure magnitudes in Kron (1980)-like apertures as well as a variety of aperture magnitudes up to  $7^{\text{m}}$ ; where the measured magnitude in a given image is below the 5-detection threshold, it is flagged by adding 100 to the measured value. Where a magnitude cannot be measured as the net flux is negative, the magnitude given is replaced with the formal 5-lim for that image and is flagged as an upper limit (this value is more appropriate than, say, the 80% completeness magnitude as we know the position at which the object would be if it could be detected). We set a minimum Kron radius equal to the seeing so that magnitudes are not measured in unphysically small apertures.

Due to the increased field of view of the U-band data, we also construct catalogs detected in the U-band (and measured from the U B V R I K s as before). A Ks-band selected catalog containing only seeing-matched R I K s magnitudes (and excluding the U B V data with poorer seeing) and with less conservative detection parameters is also generated for the purpose of studying the population of objects with very red colors (Afonso et al., in prep.).

We compare the number counts of our  $^2$ -detected catalogs in the B-band with published values from deep optical surveys as a consistency check on the counts derived from this

dataset, and to compare that the completeness limits that we have derived using simulations (presented in Table 4) are consistent with the incompleteness limits in our actual data. Figure 4 shows our B-band counts compared with the deeper counts of Metcalfe et al. (2001) and McCracken et al. (2003). Firstly, we see an excellent agreement in the counts below  $B_{AB} = 24$ , to which magnitude we can be reasonably confident our imaging is complete. Secondly, the figure illustrates that the completeness limits we derived in our simulations correspond well to the 50 and 80% limits in our actual data.

### 3.5. Radio-optical-spectroscopic identifications

We identify optical counterparts to the radio data using the final  $\chi^2$ -detected catalogs for the central three pointings, and U-band catalogs for the areas not observed in B V R I K s. There are several techniques which could be used to cross-correlate the radio and optical catalogs. One statistically robust method is the likelihood ratio method of Sutherland & Saunders (1992) (but see also, e.g., Maselli et al. 2001; Rutledge et al. 2000; Wolstencroft et al. 1986). After implementing this method, including the use of an iterative estimate for  $Q$ , the prior probability of a counterpart existing with a particular magnitude, it was found that < 1% of the potential optical counterpart galaxies differed from those found using a straightforward nearest-neighbour matching. This is not unreasonable given the relative sensitivities and positional accuracies of the 1.4 GHz and optical catalogs. When the few discrepant counterpart candidates were visually inspected they were all found to be optically faint galaxies very close to optically bright systems, where the radio position most closely matched the faint galaxy. In all such cases the most visually convincing counterpart is the fainter system. Given this result, and combined with the additional prior information required by the likelihood ratio method, (some of which, like  $Q$ , is not explicitly known), and the simplicity of the nearest-neighbour matching, we chose to use the nearest-neighbour criterion to identify the best optical counterpart candidates (Magliocchetti & Maddox 2002).

We begin, then, by identifying all optical objects within  $4''$  of a radio source. We visually inspect each of these, to further strengthen the reliability of the final optical counterpart catalog, by creating "postage" stamps in each optical bandpass for every counterpart, and overlaying each stamp (including the  $\chi^2$  detection image) with the contours from the radio image. Each of these was visually inspected to ensure that the optical detection is real and a likely optical counterpart has been identified. Multiple object counterpart cases, where more than one object lies within  $4''$ , are flagged.

A detailed breakdown of the number of radio sources observed and the number of those which were detected now follows, and is also summarised in Table 5. Of the 2148 radio

sources available after merging the two catalogs described in Hopkins et al. (2003a), 839 are located in the three optical pointings 3, 7 and 11, in regions defined as "good" by the image bad pixel masks (i.e. 839 radio objects could have been detected in optical B V R I imaging of this survey). Of these, 827 lie in "good" (i.e., not masked) regions of the CTIO U-band data. A further 236 are located in the CTIO U-band imaging not overlapped by the B V R I images. Another 256 radio sources lie within the two pointings (2 and 6) covered solely by the ESO U-band data. Finally 111 radio objects are located within the smaller area defined by the K s-band mosaic.

To summarise the counterpart matching: 673/839 (79%) of the radio detections have candidate optical counterparts in the  $\sigma^2$  images; of these 639 (76%) are detected at  $\sigma \leq 5$  in one or more filters. Taking other bandpasses individually: 569/1063 (54%) in the CTIO U-band and 53/256 (21%) in the (shallow) ESO U-band have candidate counterparts detected at  $\sigma \leq 5$  significance; 91/111 (82%) of the radio detections are detected in K s at  $\sigma \leq 5$ . In total, across all the datasets 1331 radio objects are observed, with candidate optical counterparts identified for 778 (58%). Again, these figures are summarised in Table 5. The final catalog of all 778 detected radio/optical candidate counterparts can be found in Table 6.

We show the distribution of our radio galaxies with candidate optical or U-band counterparts as a function of the radio flux in Figure 5, for those radio galaxies which were covered by our optical imaging. We see detection rates of  $> 80\%$  even in the faintest radio-flux bins, and virtually 100% for the brightest radio detections, demonstrating the effectiveness of using a  $\sigma^2$ -detected catalog. The detection rate in the U-band is lower (though still  $> 50\%$  in all radio-flux bins).

The final step is to cross-correlate the radio-optical catalog with the spectroscopic observations of the PDS carried out using the 2dF instrument on the AAT. Full details of these spectroscopic observations can be found in Georgakakis et al. (1999a) and Afonso et al. (in prep.). These spectroscopic candidates were selected using shallower optical observations than those presented in this paper, effectively limited at  $R = 22.5$ , and hence only the brighter observations have spectroscopic information available. 237 of our radio/optical matches have spectral information, also listed in Table 6 where available.

#### 4. Photometric redshift analysis

For the objects in this sample without a spectroscopic redshift, we can in principle use our extensive UBVRIKs dataset to estimate photometric redshifts.

For our analysis, we use the photometric redshift code of Connolly et al. (1995) (see

also Budavari et al. 2000). We use SED templates based on those of Coleman et al. (1980) (hereafter CWW), providing four standard SEDs (E/S0, Sbc, Scd, Im), extended in the UV and IR wavelength regions using the GISSEL98 code (e.g. Bruzual & Charlot 1993). These are "observed" SEDs, and implicitly contain an amount of dust which varies between the different galaxy classes. Rather than using these four SEDs directly, we use the method of subspace fitting (Budavari et al. 2000) to provide a large number (61) of smoothly interpolated SEDs based on the reference CWW SEDs. This supports more realistic type estimates for most of the galaxies. These new SEDs are shown in Figure 6. Our revised type-classification numbering runs from -0.1 to 1.1, with the standard CWW SEDs lying at positions 0.0 (E), 0.33 (Sbc), 0.66 (Scd), and 1.0 (Im).

We allow the possible photometric redshifts to range from 0.0 to 1.3 and also apply a very weak prior constraining the absolute magnitude range of the galaxies to  $29 < M_B < 16$ , which has the effect of eliminating photometric redshifts that produce unphysically extreme luminosities. Allowing maximum redshifts greater than 1.3 introduced a large number of false photometric redshifts close to the maximum value, as at  $z = 1.4$  the 4000Å break spectral feature moves out of the band-passes of our optical imaging and some low-redshift objects can then be spuriously fitted with photometric redshifts  $z > 1.4$ . Limiting the redshift range to 1.3 eliminated this problem. While this strategy excludes the possibility of accurately identifying the highest redshift counterparts to faint radio sources, previous studies covering smaller survey areas (e.g. Richards 2000), and basing classifications on radio spectral index and optical counterpart HST imaging, show that ~60% of the radio population to  $I_{AB} < 25$  is composed of star-forming galaxies lying at  $0 < z < 1.3$ , 20% comprising AGN/QSOs, with the remainder classified as ambiguous. Hence almost all of the star-forming systems in the 1.4GHz catalog (and which are the primary focus of our companion papers) will actually lie at  $z < 1.3$ , and only a small fraction of objects (mostly QSOs and AGNs), will be lost. (This class of object is discussed further below).

We first examine the spectroscopically observed galaxies by comparing the spectroscopic and photometric redshift. Figure 7 shows this for a sample of 116 galaxies with measured UBVRI magnitudes. The filled symbols here (including points) indicate the spectroscopic classification, while the open symbols give an estimate of the best-fitting SED template type (after "binning" the 61 subspace fitted templates into four bins, based approximately on the closest CWW-type template). As well as providing reasonable redshift estimates, the best-fitting SED is also a good indicator of the galaxy type, in the sense that spectroscopic absorption-line systems are mostly well-fit by early-type SEDs, while star-forming systems are mostly well-fit by late-type SEDs.

The reliability of the photometric redshifts can be characterised in several ways. The rms

of  $j$   $z_j = z_{\text{photo}} - z_{\text{spec}}$  is 0.1 for these 116 galaxies, over the redshift range  $0 < z < 1$ . The rms of  $j \log[(1 + z_{\text{photo}}) / (1 + z_{\text{spec}})]$  is 0.028 (implying a typical uncertainty of 7% in  $1 + z_{\text{photo}}$ ). The rms of  $j$   $z_j / (1 + z_{\text{spec}})$  is 0.065. This level of reliability in the photometric redshifts compares favourably with that of other analyses based on data with similar photometric uncertainties (Hogg et al. 1998; Fernández-Soto et al. 1999, 2001; Rowan-Robinson 2003). The relative error,  $j$   $z_j / z_{\text{spec}}$  is shown as a function of  $z_{\text{spec}}$  in Figure 8, where it is clear that the roughly constant rms uncertainty in  $z_{\text{photo}}$  with redshift translates into a smaller relative error at higher redshift. The error  $j$   $z_j$  is shown as a function of apparent B-band magnitude,  $m_B$ , in Figure 9, where it is clear that the larger absolute uncertainties in  $z_{\text{photo}}$  tend to occur for fainter galaxies due to larger photometric uncertainties.

The addition of K s-band magnitudes to the  $z_{\text{photo}}$  estimate is likely to improve the reliability somewhat, though this was harder to quantify for our sample, with only 37 objects having both spectroscopic redshifts and UBVRIK photometry. The measured uncertainties from this small sample were similar to those when using only UBVRI photometry, and a fuller analysis must await further near-IR imaging. Further experimentation established that in the absence of R-band photometry (i.e. using only UBV I magnitudes),  $z_{\text{photo}}$  estimates could still be obtained with a reliability only marginally worse than above. However, the presence of an R-I color term to correctly calibrate our I photometry to the standard system required that photometric redshifts could only be estimated for objects with both R and I photometry. Eliminating other filters significantly degraded the quality of the photometric redshifts, and as a result we calculate  $z_{\text{photo}}$  only for sources having measurements including at least UBVRI.

A brief investigation of the reliability of the templates chosen is indicated in Figure 10, showing  $(R - K_s)_{AB}$  and  $(B - R)_{AB}$  against photometric redshift. The observed colors are compared with loci indicating the color-redshift relation based on the CWW SEDs used, and also compared with SEDs containing additional reddening (Georgakakis et al. 1999a). It is clear that little or no additional reddening needs to be invoked out to  $z = 1$  to produce the observed galaxy colors for this sample.

It should be noted that the photometric redshift estimates so far described neglect the AGN or QSO population, since no spectral templates representing these systems have been added to the CWW SED set used. Adding such templates from a variety of sources was extensively explored, in an attempt to account simultaneously for both the "normal" galaxies and the AGN/QSO population. None of the small number of QSOs and narrow-line AGN in the spectroscopic sample, however, were fit better by these templates than by the CWW-style templates. For the narrow-line AGNs, the CWW-style SEDs still give rise to acceptable photometric redshifts, with the colors of such objects being fit well by early-type

galaxy SEDs (the points indicated with filled stars in Figure 7). None of the three QSOs (at  $z > 1$ ) in the spectroscopic sample were well fit by any of the SEDs explored, and typically were seen to produce erroneous photometric redshifts of  $z_{\text{photo}} > 0.1$ . The implication, then, of neglecting AGN/QSO SEDs in the photometric redshift estimation will primarily be the erroneous classification of the small QSO population as low-redshift galaxies. Further work is clearly required to identify AGN/QSOs among the faintest optical counterparts of the PDS radio sources; however as there are few such objects contributing to the total galaxy sample (at least in our existing spectroscopic sample) this systematic is likely to be small when considered in combination with the intrinsic uncertainties attached to the photometric redshifts themselves.

A final population of galaxies that is overlooked in the current photometric redshift analysis is that of the extremely red galaxies (ERGs). Preliminary estimates suggest that over 400 ERGs (defined in this case by the color criterion  $R - K_s > 5$ ) exist in the NIR imaging survey, a small fraction of which (about 20 galaxies) are identified with radio counterparts (Hopkins et al. 2003b). The current photometric redshift analysis makes no attempt to classify these red SED galaxies due to the non-detection of a large fraction of these objects in one or more of the shortest wavelength passbands, where the red colors of the SEDs makes them extremely faint. The ERG population as a whole will be treated in detail in a subsequent paper using SEDs more appropriate to the presumed ERG population (Afonso et al., in prep.).

Our final photometric redshift estimates for the full sample of galaxies containing UBVRI photometry can be found in Table 6.

## 5. General photometric properties of the sample

In this section we examine the broad photometric properties of the radio-selected sample.

### 5.1. Galaxy types

To convert the observed magnitudes into rest-frame magnitudes we must apply a k-correction (see, for example, Yoshii & Takahara 1988; Poggianti 1997). The magnitude of the k-corrections for template galaxy spectra using the range of filters in this study strongly depends on galaxy type, with early-type galaxies (ellipticals and S0s) possessing larger k-corrections in the optical passbands than galaxies with later spectra. We assign each object in our survey a k-correction by fitting the observed magnitudes to a set of appropriately

redshifted model galaxy template plates of varying type. We use the popular technique of fitting a series of template SEDs to the broadband colors available for each galaxy and use the best-fitting SED for the estimation of k-corrections in each filter, linearly interpolating between the SED types. These fits are combined by weighting inversely by the variance in the observed colors to obtain a mean best-fitting SED for each galaxy. This process was performed for the photometric-redshift sample in Section 4; here we repeat the exercise for the spectroscopic sub-sample. We use the subspace-filtered SEDs of Coleman et al. (1980) as in the photometric redshift analysis.

In Figure 11, we present the results of the fitting process, showing the distribution of the spectroscopic and photometric redshift galaxy types ( $T$ ), with  $T = 0$  representing the E SED and  $T = 1$  the Im SED. Figure 11 shows the distribution of galaxy types for the spectroscopic subsample. The mean type is  $T = 0.36$  ('Sbc) for the spectroscopic and  $T = 0.39$  for the photometric redshift galaxies. The distribution of the spectroscopic-redshift types shows an absence of blue systems due to the original R-band limited selection of the spectroscopic follow-up sample. The photometric-redshift distribution isatter, with no particular predominance of any one galaxy SED. There is also a good agreement seen between the derived types for those objects with photometric redshifts compared to spectroscopic redshifts, as shown by the dotted line in the plots.

## 5.2. Color-color diagrams

In the absence of spectroscopic information for the optically faint radio population, color-color diagrams provide a related and complementary method to that of photometric redshifts to statistically examine the physical nature of the population, as well as a comparison with standard galaxy SEDs. We present color-color diagrams, together with the predictions of the expected colors of optically faint galaxies based on the CWW SEDs, in Figure 12. This confirms that the CWW SEDs are appropriate for exploring the photometric redshifts, as they appear to adequately span the color-color space occupied by the catalogued galaxies. A detailed analysis of the colors of the radio-detected population will be explored in a subsequent paper (Sullivan et al., in prep.), also addressing the star-formation and obscuration properties of the optically-detected galaxies from the 1.4 GHz catalog.

### 5.3. Distribution by type

There is a trend in Figure 12 for the lower 1.4 GHz flux density objects to preferentially lie in the region of color-color space described best by later-type SEDs. This is explored more explicitly in Figure 13, showing histograms of  $S_{1.4}$  for four bins in best-fitting SED type, based on the photometric redshift results. It is clear that the lower flux densities have an increasing proportion of later-type SEDs, consistent with earlier results (e.g., Benn et al. 1993; Windhorst et al. 1985). Figure 14 shows histograms of  $S_B = S_{1.4}$  split by best-fitting SED type. Systems with higher  $S_B = S_{1.4}$  ratios are also seen to be dominated by later-type SEDs, illustrating the larger apparent contribution of late-types at lower 1.4 GHz flux densities, as the distribution of  $S_B$  is fairly uniform over all SED types. Clearly there are complex selection effects at work which affect these distributions which will be analysed further in our later papers.

## 6. Summary

In this paper, we have presented complementary optical UBVRIK imaging to the Phoenix Deep Survey (PDS; Hopkins et al. 2003a). The optical UBVRI imaging covers an area on the sky of  $\sim 1$  square degree to  $R \sim 24.5$ , with a smaller sub-region of near-IR Ks data. Within this optical imaging, 778 radio sources can be assigned candidate optical counterparts. We have explored photometric redshift calculation techniques and present these estimates for each of the candidate optical counterparts. These, in combination with the catalogs and data described above, will be used to support future detailed analyses of the PDS galaxies.

The authors would like to thank Andrew Connolly and David Gilbank for useful discussion. M.S. acknowledges support from a PPARC fellowship. A.M.H. acknowledges support provided by the National Aeronautics and Space Administration (NASA) through Hubble Fellowship grant HST-HF-01140.01-A awarded by the Space Telescope Science Institute (STScI). J.A. gratefully acknowledges the support from the Science and Technology Foundation (FCT, Portugal) through the fellowship BPD-5535-2001 and the research grant POCI-FNU-43805-2001. Based on observations obtained at Cerro Tololo Inter-American Observatory a division of the National Optical Astronomy Observatory, which is operated by the Association of Universities for Research in Astronomy, Inc. under cooperative agreement with the National Science Foundation. Based on data acquired with the Wide-Field Imager at the Anglo-Australian Observatory. Based on observations made with ESO Telescopes at the La Silla Observatory under program me ID s 66 A -0193 and 67 A -0403.

R E F E R E N C E S

- A delberger, K . L . & Steidel, C . C . 2000, ApJ, 544, 218
- Afonso, J ., Hopkins, A ., Mobasher, B ., & Elmehdai, C . 2003, in press, ApJ, astro{ph/0307175
- Bell, E . F . 2003, ApJ, 586, 794
- Benn, C . R ., Rowan-Robinson, M ., McMahon, R . G ., Broadhurst, T . J ., & Lawrence, A . 1993, MNRAS, 263, 98
- Bertin, E . & Arnouts, S . 1996, A & AS, 117, 393
- Bessell, M . S . 1990, PASP, 102, 1181
- Bruzual, A . G . & Charlot, S . 1993, ApJ, 405, 538
- Buat, V ., Boselli, A ., Gavazzi, G ., & Bonfanti, C . 2002, A & A, 383, 801
- Budavari, T ., Szalay, A . S ., Connolly, A . J ., Csabai, I ., & Dickinson, M . 2000, AJ, 120, 1588
- Calzetti, D . 2001, PASP, 113, 1449
- Coleman, G . D ., Wu, C . ., & Woodward, D . W . 1980, ApJS, 43, 393
- Condon, J . J . 1992, ARA&A, 30, 575
- Condon, J . J ., Anderson, M . L ., & Helou, G . 1991, ApJ, 376, 95
- Condon, J . J ., Cotton, W . D ., & Broderick, J . J . 2002, AJ, 124, 675
- Connolly, A . J ., Csabai, I ., Szalay, A . S ., Koo, D . C ., Kron, R . G ., & Gunn, J . A . 1995, AJ, 110, 2655
- Connolly, A . J ., Szalay, A . S ., Dickinson, M ., Subbarao, M . U ., & Brunner, R . J . 1997, ApJ, 486, L11
- de Jong, T ., Klein, U ., Wielebinski, R ., & Wunderlich, E . 1985, A & A, 147, L6
- Fernandez-Soto, A ., Lanzetta, K . M ., Chen, H ., Pascarelle, S . M ., & Yahata, N . 2001, ApJS, 135, 41
- Fernandez-Soto, A ., Lanzetta, K . M ., & Yahil, A . 1999, ApJ, 513, 34
- Fukugita, M ., Shimasaki, K ., & Ichikawa, T . 1995, PASP, 107, 945

- Gomez, P. L., Nichol, R. C., Miller, C. J., Balogh, M. L., Goto, T., Zabludo, A. I., Romer, A. K., Bernardi, M., Sheth, R., Hopkins, A. M., Castander, F. J., Connolly, A. J., Schneider, D. P., Brinkmann, J., Lamb, D. Q., Subbarao, M., & York, D. G. 2003, ApJ, 584, 210
- Georgakakis, A., Mobasher, B., Cram, L., Hopkins, A., Lidman, C., & Rowan-Robinson, M. 1999a, MNRAS, 306, 708
- Georgakakis, A., Mobasher, B., Cram, L., Hopkins, A., & Rowan-Robinson, M. 2000, A&AS, 141, 89
- Georgakakis, A. E., Mobasher, B., Cram, L., & Hopkins, A. 1999b, MNRAS, 310, L15
- Haarsma, D. B., Partridge, R. B., Windhorst, R. A., & Richards, E. A. 2000, ApJ, 544, 641
- Hogg, D. W., Cohen, J. G., Blaizot, R., Gwyn, S. D. J., Hartwick, F. D. A., Mobasher, B., Mazzei, P., Sawicki, M., Lin, H., Yee, H. K. C., Connolly, A. J., Brunner, R. J., Sabai, I., Dickinson, M., Subbarao, M. U., Szalay, A. S., Fernández-Soto, A., Lanzetta, K. M., & Yahil, A. 1998, AJ, 115, 1418
- Hopkins, A., Georgakakis, A., Cram, L., Afonso, J., & Mobasher, B. 2000a, ApJS, 128, 469
- Hopkins, A. M., Afonso, J., Chan, B., Cram, L. E., Georgakakis, A., & Mobasher, B. 2003a, AJ, 125, 465
- Hopkins, A. M., Afonso, J., Georgakakis, A., Sullivan, M., Mobasher, B., & Cram, L. E. 2003b, in "Multiwavelength Cosmology Conference", Mykonos Island, astro-ph/0309147
- Hopkins, A. M., Connolly, A. J., Haarsma, D. B., & Cram, L. E. 2001, AJ, 122, 288
- Hopkins, A. M., Connolly, A. J., & Szalay, A. S. 2000b, AJ, 120, 2843
- Hopkins, A. M., Miller, C. J., Nichol, R. C., Connolly, A. J., Bernardi, M., Gomez, P. L., Goto, T., Tremonti, C. A., Brinkmann, J., & Lamb, D. Q. 2003c, in press, ApJ, astro-ph/0306621
- Kron, R. G. 1980, ApJS, 43, 305
- Landolt, A. U. 1992, AJ, 104, 340
- Lilly, S. J., Le Fevre, O., Hammer, F., & Crampton, D. 1996, ApJ, 460, L1

- Madau, P., Ferguson, H. C., Dickinson, M. E., Giavalisco, M., Steidel, C. C., & Fruchter, A. 1996, MNRAS, 283, 1388
- Magliocchetti, M. & Maddox, S. J. 2002, MNRAS, 330, 241
- Masch, F. J., Condon, J. J., Barlow, T. A., Lonsdale, C. J., Xu, C., Shupe, D. L., Pevunova, O., Fang, F., & Cutri, R. 2001, PASP, 113, 10
- McCracken, H. J., Radovich, M., Bertin, E., Mellier, Y., Dantel-Fort, M., LeFevre, O., Cuillandre, J. C., Gwyn, S., Foucaud, S., & Zamorani, G. 2003, in press, A&A, astro-ph/0306254
- Metcalf, N., Shanks, T., Campos, A., McCracken, H. J., & Fong, R. 2001, MNRAS, 323, 795
- Mobasher, B., Cram, L., Georgakakis, A., & Hopkins, A. 1999, MNRAS, 308, 45
- Oke, J. B. 1974, ApJS, 27, 21
- Persson, S. E., Murphy, D. C., Kozemianski, W., Roth, M., & Rielle, M. J. 1998, AJ, 116, 2475
- Poggianti, B. M. 1997, A&AS, 122, 399
- Richards, E. A. 2000, PASP, 112, 1001
- Rowan-Robinson, M. 2003, MNRAS, 345, 819
- Rutledge, R. E., Brunner, R. J., Prince, T. A., & Lonsdale, C. 2000, ApJS, 131, 335
- Smail, I., Owen, F. N., Morrison, G. E., Keel, W. C., Ivison, R. J., & Ledlow, M. J. 2002, ApJ, 581, 844
- Sullivan, M., Mobasher, B., Chan, B., Cram, L., Ellis, R., Treier, M., & Hopkins, A. 2001, ApJ, 558, 72
- Sullivan, M., Treier, M. A., Ellis, R. S., Bridges, T. J., Willard, B., & Donas, J. 2000, MNRAS, 312, 442
- Sutherland, W. & Saunders, W. 1992, MNRAS, 259, 413
- Szalay, A. S., Connolly, A. J., & Szokoly, G. P. 1999, AJ, 117, 68
- Tresse, L. & Maddox, S. J. 1998, ApJ, 495, 691

- Tresse, L., Maddox, S. J., Le Fèvre, O., & Cuby, J.-G. 2002, MNRAS, 337, 369
- Valdes, F. G. 1998, in ASP Conf. Ser. 145: Astronomical Data Analysis Software and Systems VII, Vol. 7, 53
- Windhorst, R. A., Miley, G. K., Owen, F. N., Kron, R. G., & Koo, D. C. 1985, ApJ, 289, 494
- Wolstencroft, R. D., Savage, A., Clowes, R. G., MacGillivray, H. T., Leggett, S. K., & Kalas, M. 1986, MNRAS, 223, 279
- Yoshii, Y. & Takahara, F. 1988, ApJ, 326, 1

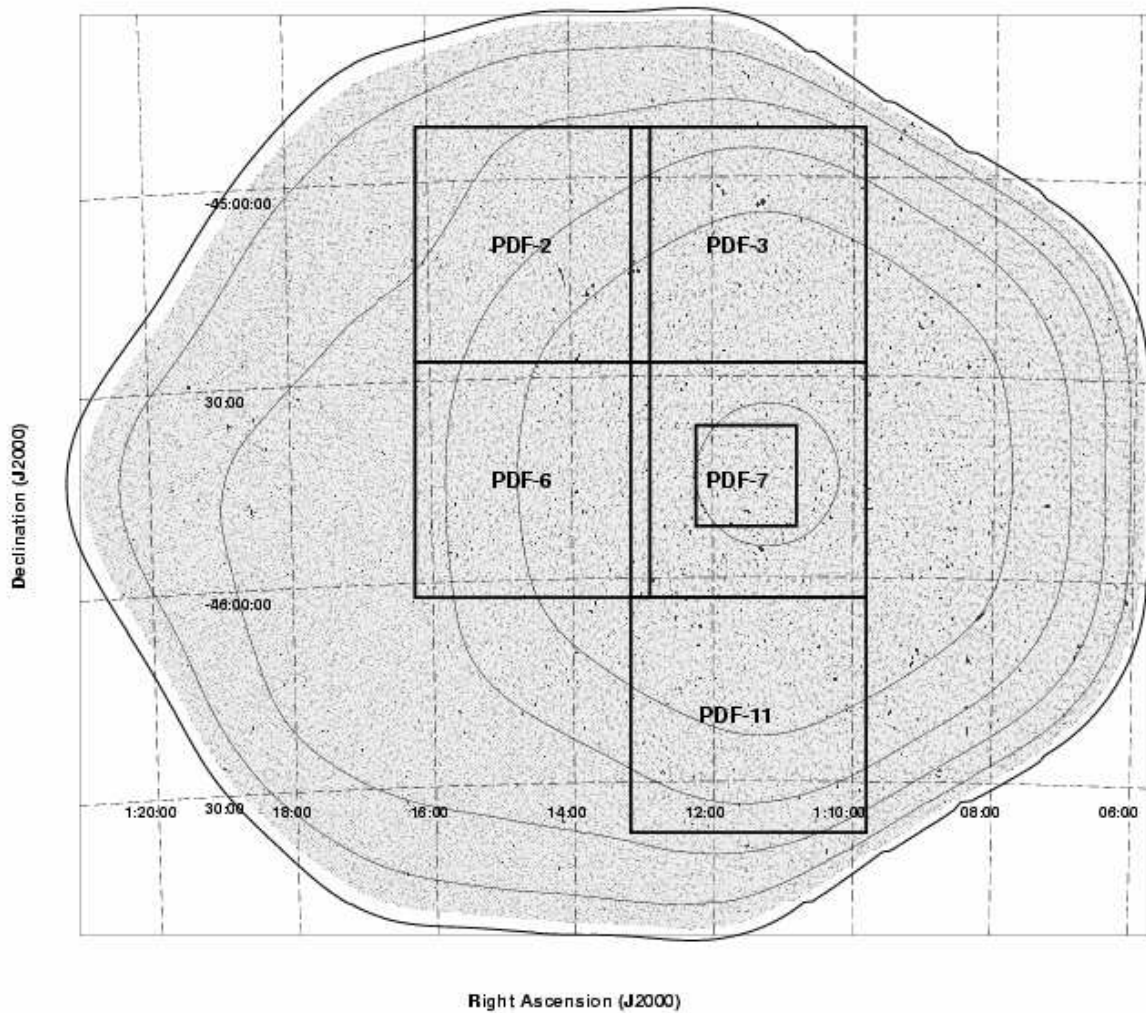


Fig. 1. | The optical masking pattern of the PDS overlaid on the full 1.4 GHz ATCA radio map. Contours show the theoretical rms noise level over the radio mosaic, ranging from 10 Jy (inner circle) to 0.32 mJy, in steps of factors of 2. The large rectangular boxes show the location of each optical masking pointing and the associated numbering system. The small rectangle denotes the extent of the Ks data.

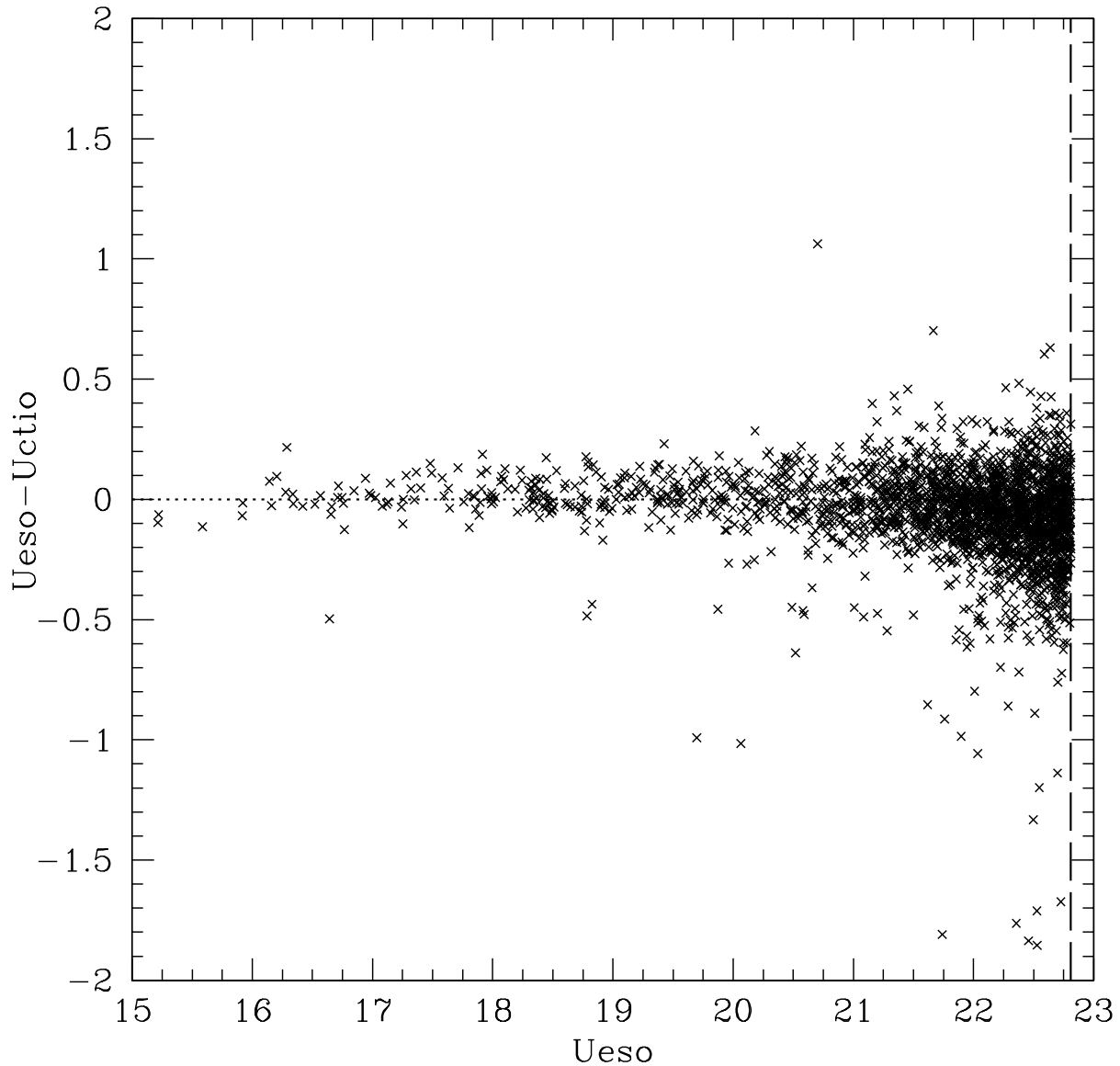
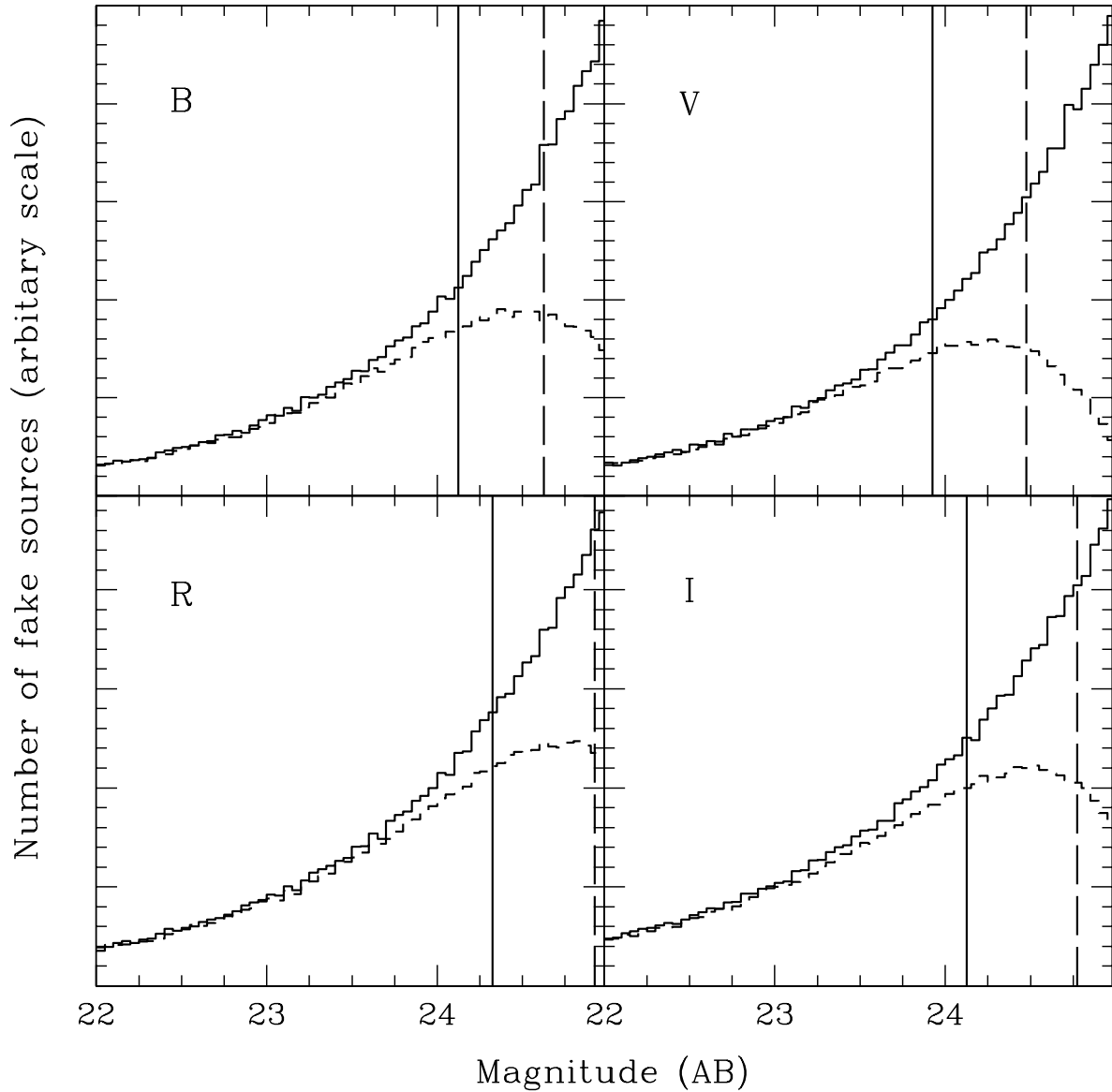


Fig. 2. | A comparison of 3<sup>00</sup> aperture magnitudes for common objects between the CTIO and ESO U-band data, shown as the difference in the magnitudes as a function of the ESO magnitude. The vertical dashed line shows the limiting magnitude of the ESO data. The figure demonstrates an excellent agreement between U-band data taken at different sites with different telescopes/instruments.



**Fig. 3.** Example simulations of the optical completeness limits for the central pointing of the PDF survey (pointing PDF-7 in Fig. 1). Solid curves denote the cumulative counts for "fake" sources placed into the images; the broken curve shows the fraction recovered as a function of magnitude. The vertical solid and dashed lines show 80% and 50% completeness magnitudes respectively. See text for details of the simulations.

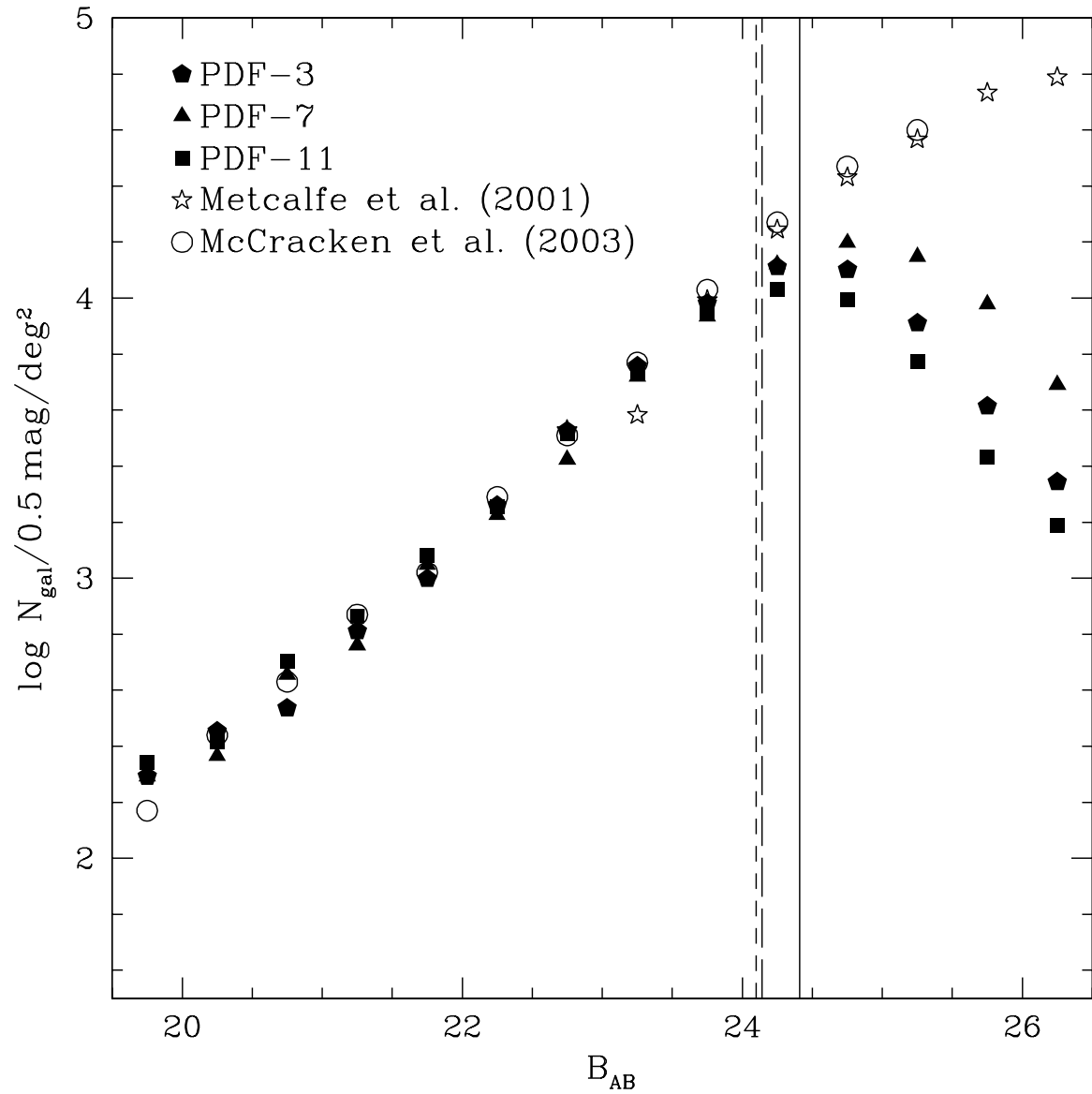


Fig. 4.| The  $B_{AB}$  number counts (derived from sextractor magauto magnitudes) for the 3 central pointings in our optical data, together with the  $B$ -band counts of Metcalfe et al. (2001) and McCracken et al. (2003). The vertical lines show the 80% completeness limits for PD S-7 (solid line), PD S-3 (long-dashed line) and PD S-11 (short-dashed line).

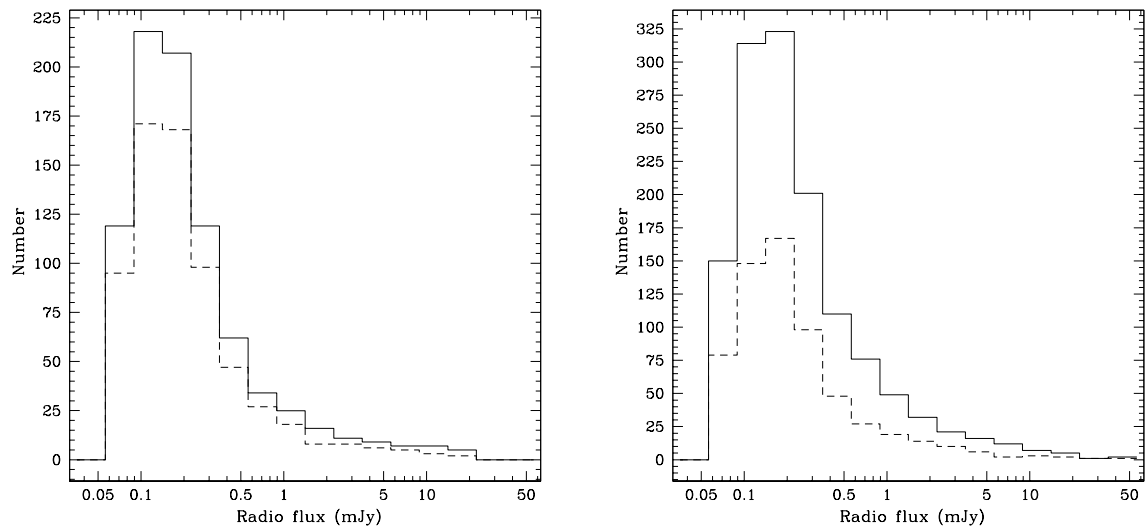


Fig. 5. | The distribution of radio/optical (left) and radio/U-band (right) candidate matches as a function of radio flux. The solid lines show the flux distribution of all radio sources, the dashed lines show the flux distribution of the candidate counterparts.

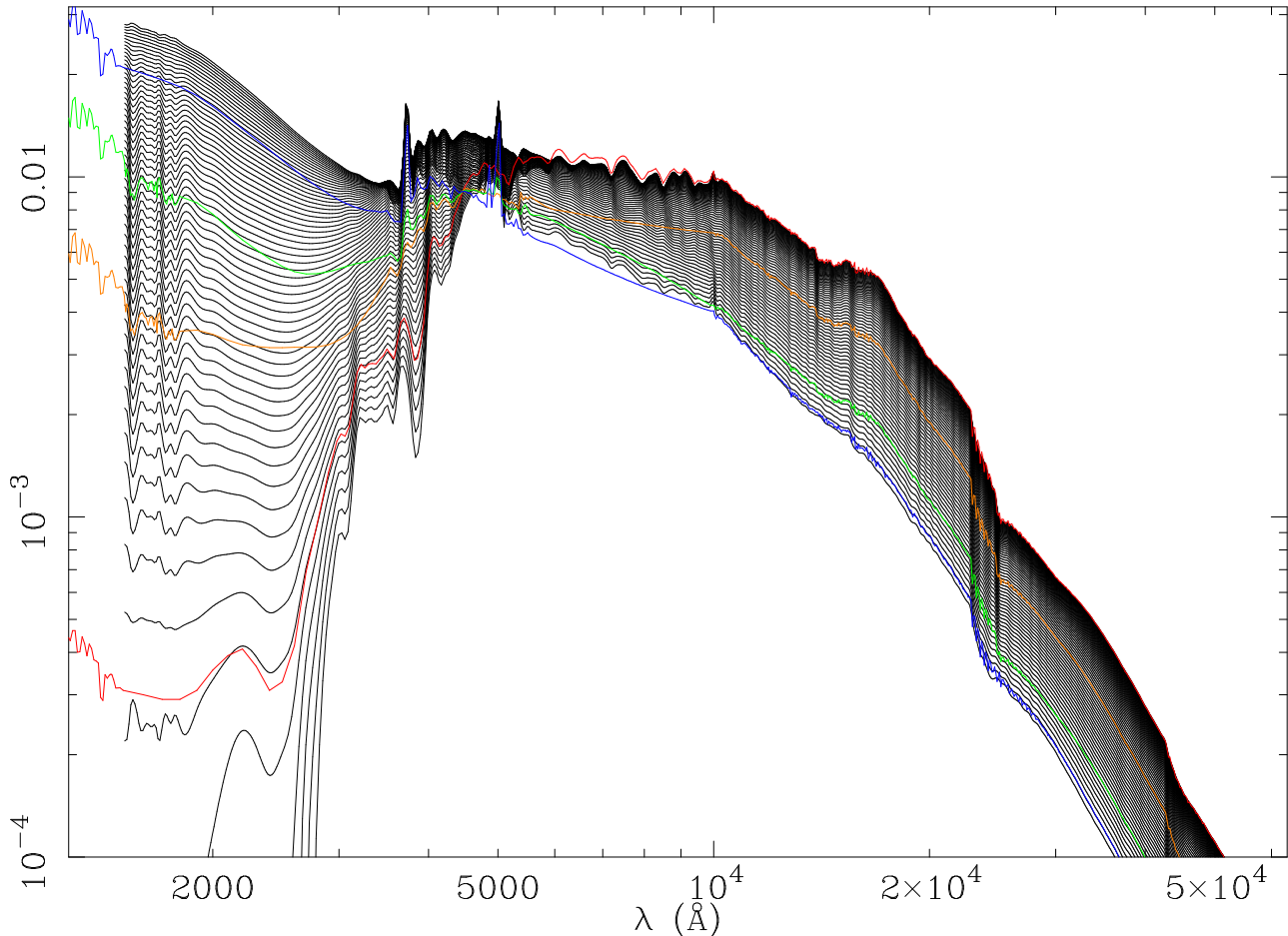
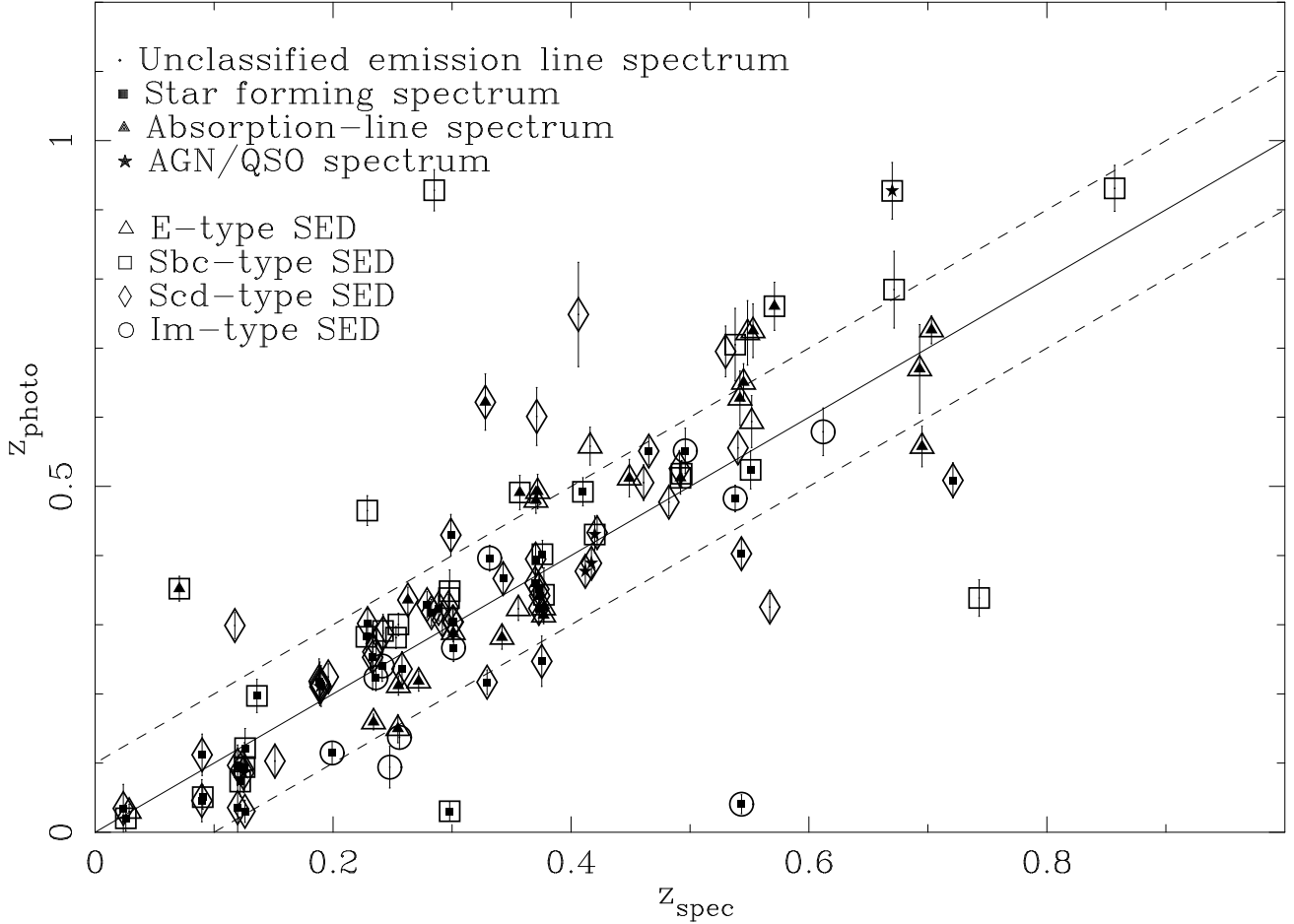


Fig. 6.| The 61 subspace iterated SEDs shown with the 4 original CW W SED templates overlaid. Red: E-type (0.0); Orange: Sbc-type (0.33); Green: Scd-type (0.67); Blue: Im-type (1.0).



**Fig. 7.** A comparison of spectroscopic and photometric redshifts for the spectroscopically-observed subsample. The points and filled symbols refer to the spectroscopic classification of the galaxies (Georgakakis et al. 1999a), while the open symbols refer to the best-fitting SED from the photometric redshift estimation. The open symbols should be treated as a rough guide only, since they group the 61 subspace fitted SEDs into the closest CW W-type classification, with SEDs from  $-0.10 \{ 0.20$  called E-type,  $0.21 \{ 0.50$  Sbc-type,  $0.51 \{ 0.80$  Scd-type and  $0.81 \{ 1.10$  Im-type. Note that this figure shows redshift in linear units, with the dashed lines indicating offsets of 0.1 in  $z_{\text{photo}}$  about the one-to-one line.

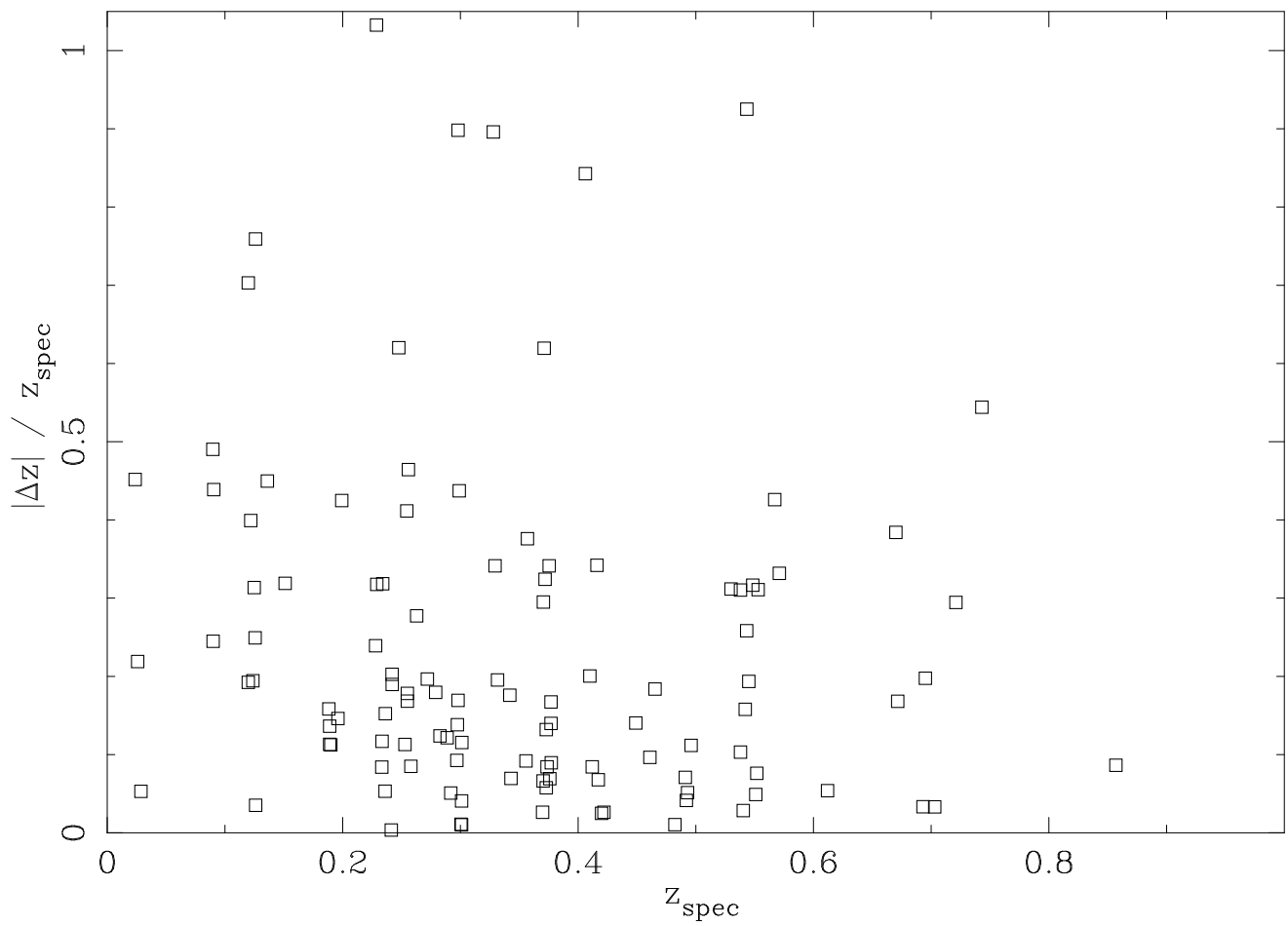


Fig. 8. | Distribution of  $|\Delta z| / z_{\text{spec}}$  with spectroscopic redshift.

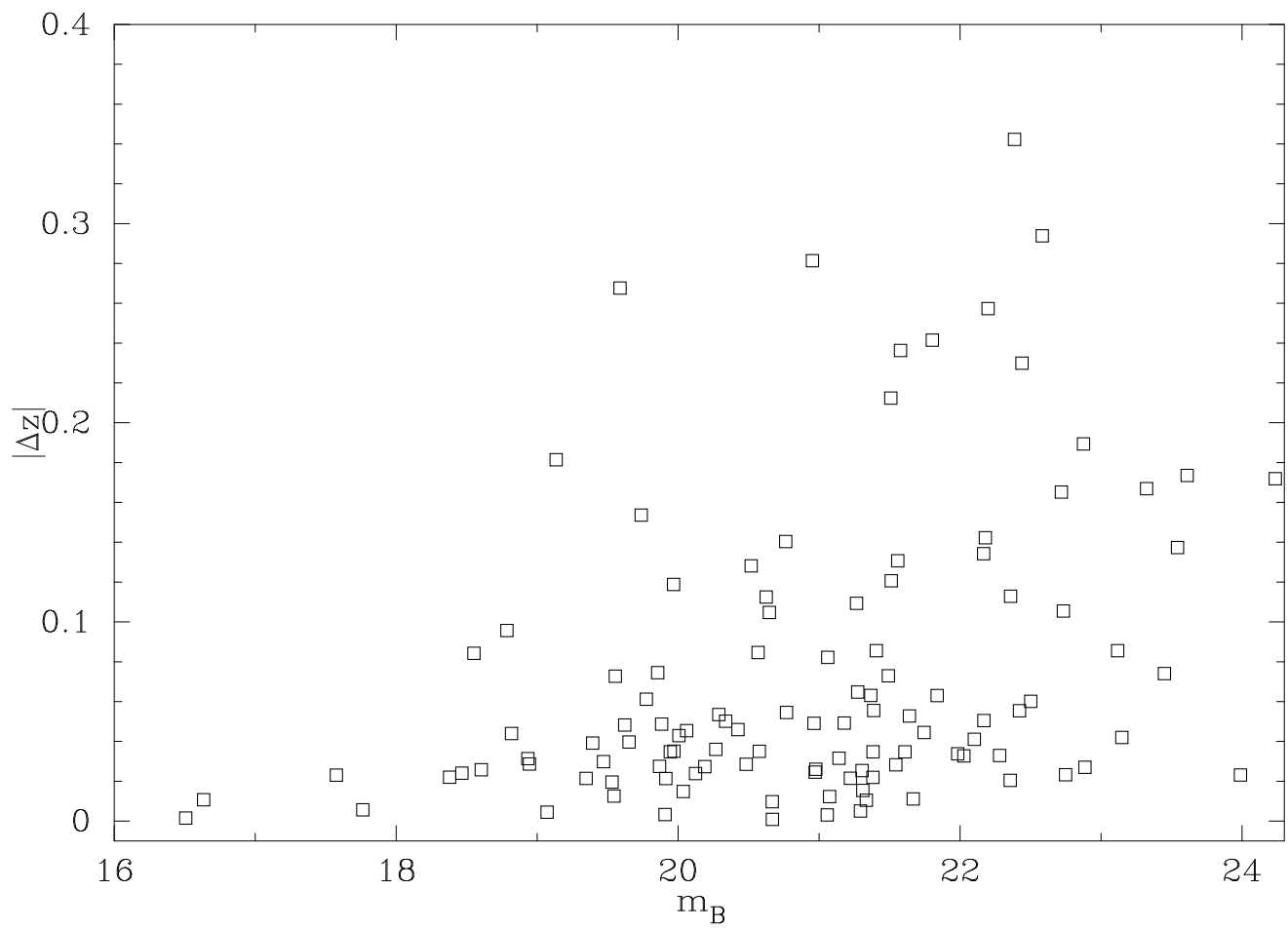


Fig. 9. Distribution of  $z$  with B-band magnitude, showing that (as expected) photo-metric redshift uncertainties increase for fainter systems.

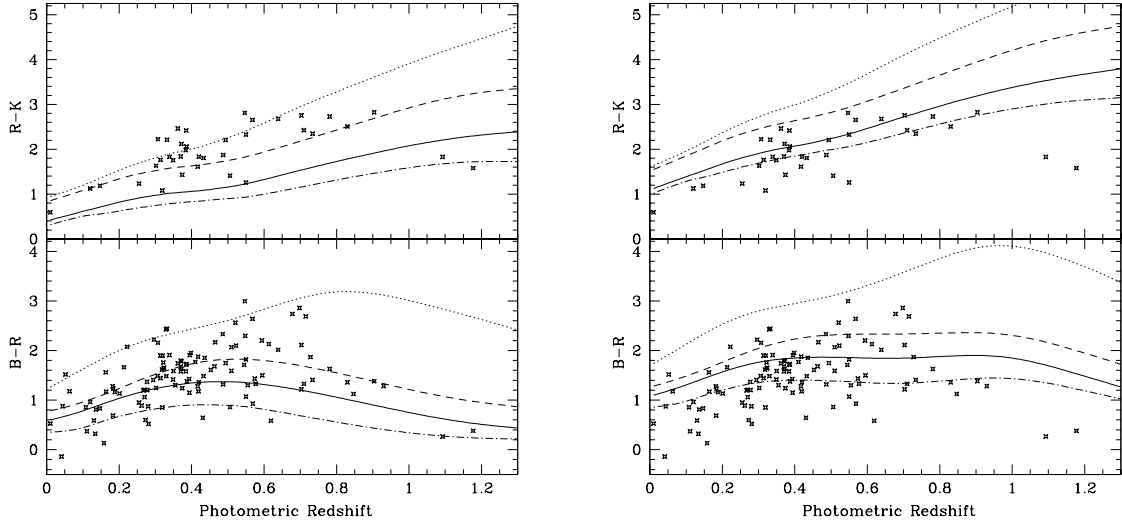


Fig. 10. |  $R_{AB} - K_{SAB}$  (UPPER) and  $B_{AB} - R_{AB}$  (LOWER) as a function of redshift, compared with the colors corresponding to the SEDs used in the photometric redshift estimation. Both panels show SED colors for the 4 CW W-type SEDs used (upper SED to lower SED these are E : dotted, Sbc: dashed, Scd: solid, Im : dot-dashed). The curves in the right-hand panel have additional reddening ( $A_V = 1.0$ ) compared to the templates used for deriving photometric redshifts.

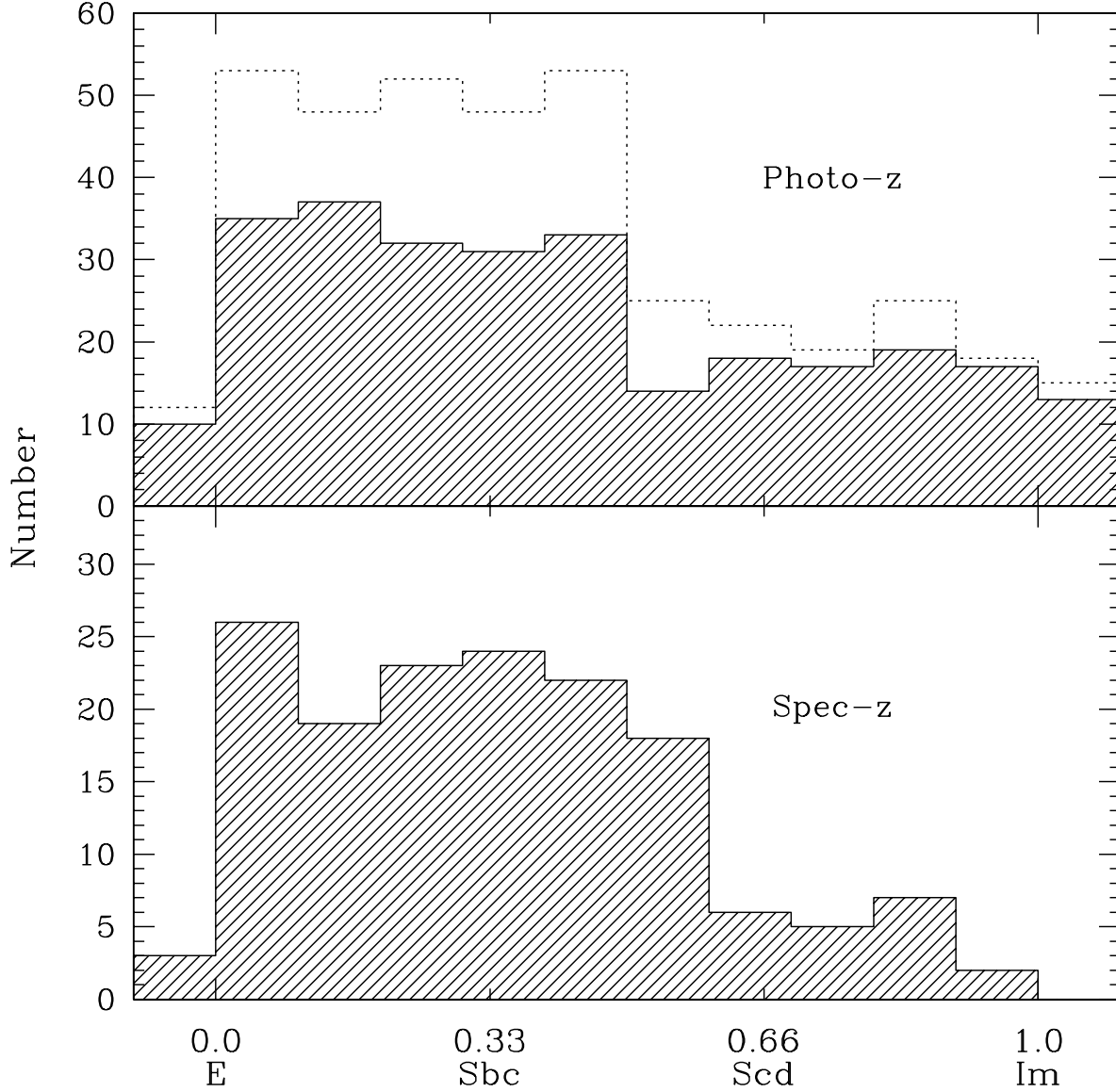
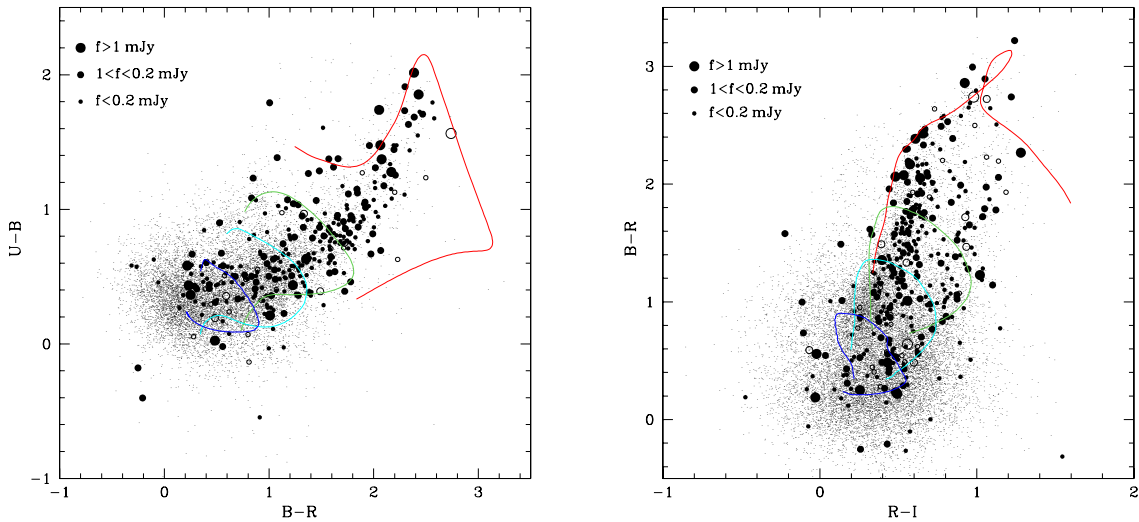


Fig. 11. The distribution of galaxy types for the sub-sample with spectroscopic (lower) and photometric (upper) redshifts calculated using the CWW SEDs. The dotted line in the photometric-redshift type distribution shows the location of those galaxies with a spectroscopic redshift for which a photometric estimate has also been estimated. The median type for both samples is approximately an Sbc SED. No dust is added to the CWW SEDs in this analysis. Galaxies spectroscopically classified as AGN are omitted from this analysis.



**Fig. 12.** Color-color diagrams for the radio population compared to objects in the field as a whole. Radio objects are marked as circles where the size denotes the radio flux of the source according to the key. Filled circles are radio objects with single optical counterparts within  $3''$ , open circles are objects with more than one optical counterpart within this radius. The overlaid lines represent the position in color-color space of the CW W SED used to determine the photometric redshift estimates placed between a redshift of 0 and 1.3.

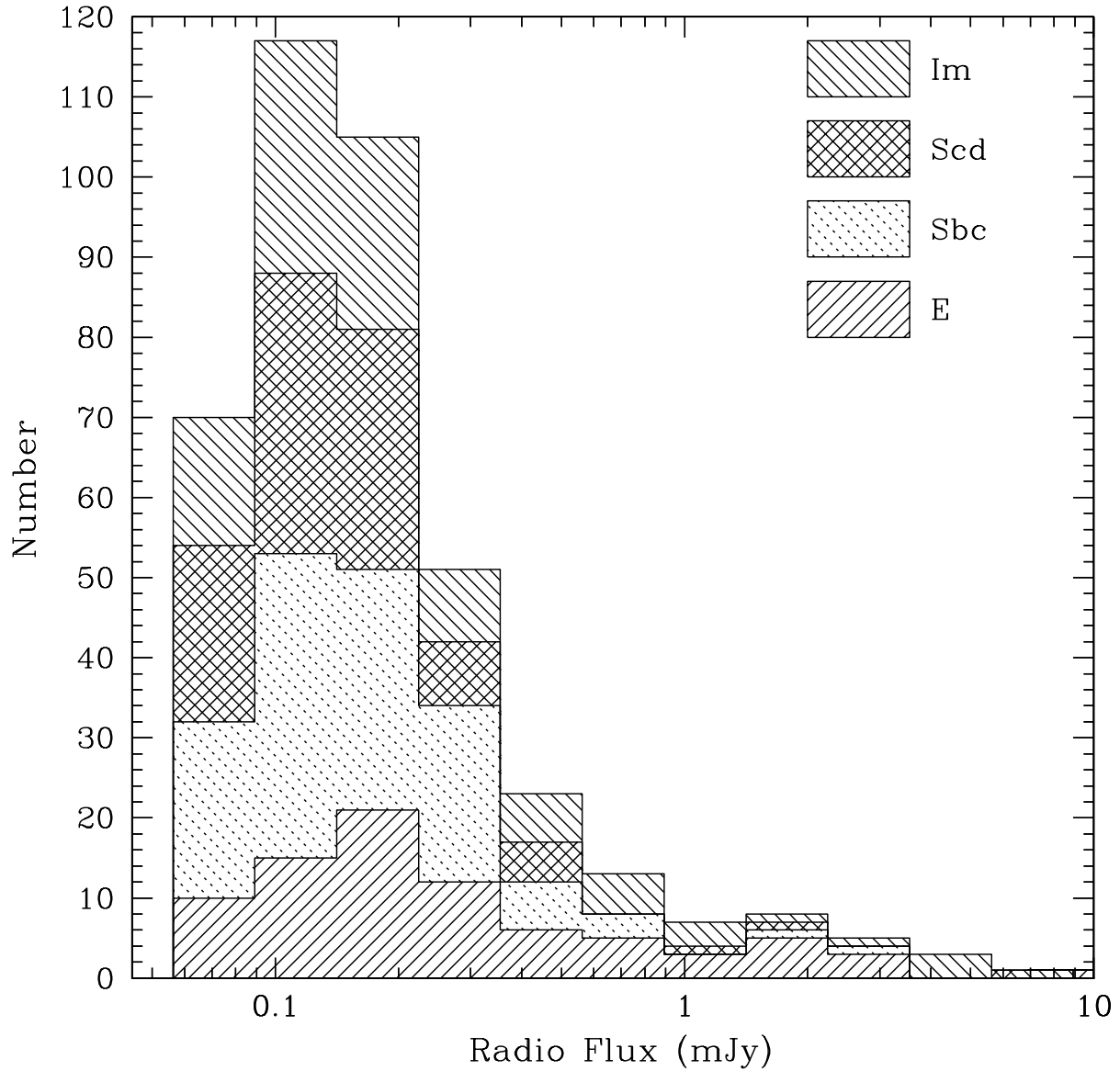


Fig. 13. Histogram showing distribution in  $S_{14}$  by best-fitting photometric redshift SED type. The four type bins are as described in the caption of Figure 7, with E-type galaxies at the bottom of the plot moving through Sb and Sc types to Im-type galaxies at the top.

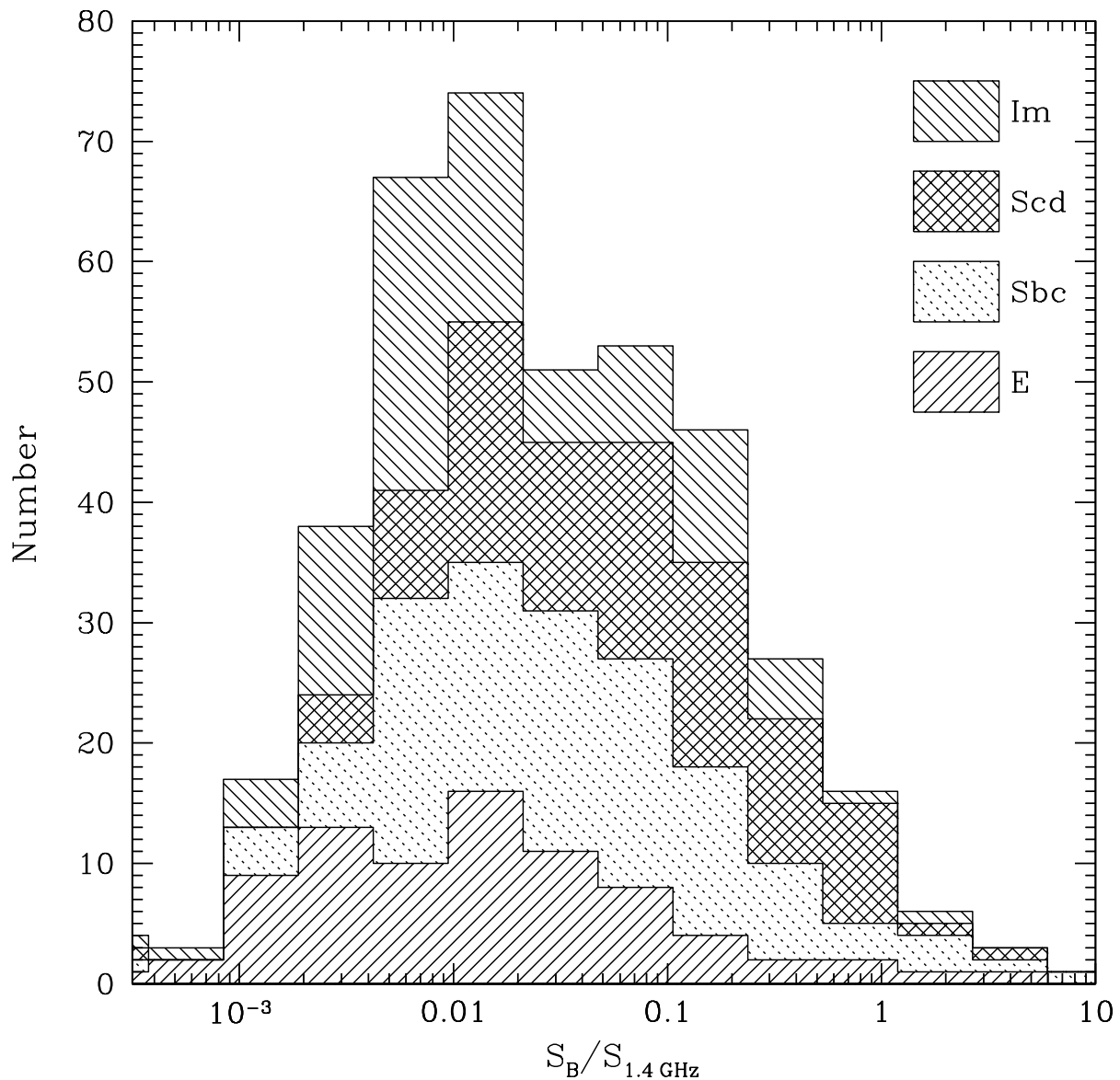


Fig. 14. | Distributions of optical ( $m_B$ ) to 1.4 GHz flux ratio, divided by type. Best-fitting SED types as in previous Figure.

Table 1. Positions of the PDS-optical pointings from Figure 1 and exposure times.

Pointing	R A (J2000)	D E C (J2000)	U <sup>a</sup>	B	V	R	i	K
2	01:14:32	-45:10:20	8 420s					
3	01:11:29	-45:10:20	5 1200s	5 480s	10 240s	8 240s	8 480s	
6	01:14:32	-45:45:30	13 240s					
7	01:11:29	-45:45:30	6 1200s	10 480s	7 300s	10 480s	15 480s	2700s-10800s
11	01:11:29	-46:20:20	6 1200s	5 480s	5 480s		2 300s	

<sup>a</sup> Pointings 3,7,11 were observed with MOSAIC-II on the CTIO 4m ; pointings 2,6 with WFI on the ESO 2.2m

Table 2. Values used to convert Vega magnitudes to the AB system<sup>a</sup>.

U	B	V	R	I	K
+ 0.883	-0.098	+ 0.011	+ 0.191	+ 0.426	+ 1.866

<sup>a</sup>Conversions listed in the sense  $m_{AB} = m_{VEGA} + C$ .

Table 3:5- Limiting magnitudes and seeing estimates for the PDS.

Pointing	U		B		V		R		I		K	
	5-	Seeing <sup>b</sup>	5-	Seeing								
3	24.78	1.32	24.64	1.50	24.30	1.45	24.00	1.49	24.39	1.42		
7	25.10	1.22	24.95	1.53	24.32	1.48	24.61	1.21	24.67	1.20	21.92	0.97
11	25.11	1.17	24.55	1.45	24.52	1.12				22.84	1.26	

<sup>a</sup>A llmagnitudes are listed in the AB system and are magauto sextractor magnitudes<sup>b</sup>Seeing estimates are given in arcseconds

Table 4: Completeness magnitudes for the various optical/near-IR pointings

Pointing	U		B		V		R		I		K	
	80%	50%	80%	50%	80%	50%	80%	50%	80%	50%	80%	50%
3	24.40	24.98	24.14	24.59	23.99	24.51	23.86	24.28	23.90	24.43		
7	24.72	25.32	24.41	24.83	23.92	24.47	24.32	24.92	24.13	24.77	21.47	22.02
11	24.67	25.30	24.10	24.50	24.03	24.58			22.76	23.07		

Table 5. The results of cross-correlating the  $\alpha^2$  and U-band catalogs.

Dataset	Number of radio objects observed	Number of radio objects detected
Optical ( $\alpha^2$ )	839	659 (79%)
U-CTIO	1063	569 (54%)
U-ESO	256	53 (21%)
K-band	111	91 (82%)
Total <sup>a</sup>	1331	778 (58%)

<sup>a</sup>Includes all independently observed radio sources in all imaging campaigns

Table 6. Photometric data for the radio/optical identifications

ID	U	B	V		R		I	K	$z_{\text{spec}}$	$z_{\text{phot}}$	
PD SJ010922.1-451402		23.48	0.11	23.38	0.18	23.38	0.15	23.62	0.20		
PD SJ010926.9-450627		20.14	0.02	19.99	0.02	19.92	0.02	19.94	0.02		
PD SJ010927.0-452121		18.80	0.02	17.98	0.02	17.71	0.02	17.55	0.02	0.172	
PD SJ010932.3-450444		19.46	0.02	18.47	0.02	18.14	0.02	17.99	0.02		
PD SJ010934.9-451646		24.40	0.17	24.00	0.16	23.99	0.12	24.05	0.14		
PD SJ010935.4-451301		24.78	0.31	23.90	0.25	23.64	0.16	23.01	0.11		
PD SJ010935.4-451853	> 24.98	23.72	0.20	23.15	0.17	22.96	0.11	23.08	0.13		
PD SJ010935.6-460620	23.70	0.22				> 24.67					
PD SJ010937.7-462038	22.79	0.07				> 24.67					
PD SJ010939.4-455115	24.50	0.16									
PD SJ010941.7-460131	24.28	0.14									
PD SJ010942.6-461509	24.84	0.28			23.39	0.12					
PD SJ010943.0-451655	125.28	0.55	23.90	0.17	23.33	0.13	23.21	0.10	22.65	0.07	0.20 0:04
PD SJ010943.7-460137	19.19	0.02									0.120
PD SJ010943.8-454150	125.40	0.49	125.78	0.56	124.92	0.49	24.09	0.12	23.26	0.10	1.28 0:31
PD SJ010943.9-461019	23.04	0.08	22.56	0.08	21.46	0.04					
PD SJ010944.0-453845	20.31	0.02	19.74	0.02	19.36	0.02	19.37	0.02	19.07	0.02	0.248 0.11 0:01
PD SJ010944.2-454959	24.22	0.20	24.65	0.28	23.92	0.31	23.29	0.12	22.50	0.09	0.90 0:24
PD SJ010944.8-455817	21.38	0.02	20.23	0.02	19.04	0.02	18.58	0.02	18.00	0.02	0.32 0:03
PD SJ010944.9-455516	23.79	0.13	23.54	0.15	23.08	0.18	22.58	0.08	21.43	0.04	0.93 0:06
PD SJ010946.3-462048	23.81	0.11	23.60	0.13	23.30	0.12					> 23.05
PD SJ010946.4-455002	24.59	0.30	22.73	0.05	21.17	0.02	20.15	0.02	19.16	0.02	0.545 0.68 0:04
PD SJ010946.5-454657	17.20	0.02	15.83	0.02	15.08	0.02					
PD SJ010946.6-453253	23.57	0.07	22.88	0.03	22.48	0.04	21.91	0.02	21.39	0.02	0.71 0:04
PD SJ010947.9-455125	17.44	0.02	16.10	0.02	15.42	0.02					0.020
PD SJ010948.1-460352	24.06	0.15	24.03	0.15	23.63	0.13					> 23.05
PD SJ010949.2-454031	24.62	0.27	23.61	0.10	21.97	0.04	20.95	0.02	20.01	0.02	0.548 0.70 0:06
PD SJ010949.4-451741	24.97	0.38	24.40	0.28	23.74	0.15	23.99	0.18	23.55	0.17	0.24 0:05
PD SJ010949.4-461351	23.40	0.08	22.09	0.03	20.72	0.02			19.45	0.02	
PD SJ010950.0-453713	> 25.30		> 25.30		> 24.62		23.02	0.10	21.53	0.04	
PD SJ010950.1-454628	20.73	0.02	19.91	0.02	18.95	0.02	18.62	0.02	18.16	0.02	0.300 0.35 0:02
PD SJ010950.4-460116	21.41	0.02									0.550
PD SJ010951.6-455611	125.97	0.21	24.10	0.09	23.23	0.09	22.88	0.08	22.38	0.07	0.22 0:03
PD SJ010951.8-455004	23.43	0.06	22.72	0.03	22.07	0.03	21.55	0.02	20.90	0.02	0.530 0.70 0:04
PD SJ010951.9-454557	21.63	0.02	20.98	0.02	20.19	0.02	19.98	0.02	19.62	0.02	0.33 0:03
PD SJ010951.9-455809	25.22	0.37	24.39	0.20	22.67	0.07	21.76	0.02	20.77	0.02	0.73 0:05
PD SJ010952.1-451748	23.79	0.12	22.78	0.06	21.49	0.02	21.03	0.02	20.46	0.02	0.18 0:03
PD SJ010952.4-452044	> 24.98		> 24.92		24.58	0.37	23.82	0.16	22.61	0.09	
PD SJ010952.7-453035	21.44	0.02	20.42	0.02	19.37	0.02	18.99	0.02	18.44	0.02	0.242 0.33 0:02
PD SJ010952.7-454415	24.44	0.24	24.11	0.17	24.49	0.47	23.70	0.13	22.73	0.09	0.93 0:12
PD SJ010953.4-462930	24.70	0.25	23.39	0.13	21.80	0.03			20.52	0.04	
PD SJ010953.5-450156	24.34	0.30	22.10	0.04	20.63	0.02	19.73	0.02	19.10	0.02	0.33 0:02
PD SJ010954.0-454633	125.77	0.49	24.69	0.17	23.17	0.08	22.12	0.02	21.21	0.02	0.72 0:09
PD SJ010954.6-460552	16.54	0.02	15.36	0.02	14.66	0.02			14.22	0.02	0.024
PD SJ010954.6-445523			23.16	0.07	22.78	0.09	22.76	0.08	22.72	0.09	
PD SJ010954.9-453341	23.17	0.10	21.63	0.02	20.14	0.02	19.50	0.02	18.84	0.02	0.28 0:02
PD SJ010955.2-455816	> 25.30		> 25.30		24.40	0.29	125.34	0.48			
PD SJ010955.2-455918	125.59	0.52	25.01	0.37	23.42	0.14	22.44	0.04	21.33	0.02	0.69 0:11
PD SJ010955.2-453100	22.87	0.08	21.28	0.02	19.88	0.02	19.01	0.02	18.25	0.02	0.52 0:02

Table 6 | Continued

ID	U	B	V	R	I	K	$z_{\text{spec}}$	$z_{\text{phot}}$				
PD SJ010955.2-455812	23.52	0.08	22.68	0.04	21.75	0.03	21.01	0.02	20.37	0.02	0.59	0:03
PD SJ010955.7-455157	24.27	0.18	23.71	0.10	23.09	0.12	22.71	0.06	22.27	0.05	0.58	0:11
PD SJ010955.7-454819	125.48	0.56	24.24	0.18	24.47	0.43	22.83	0.07	22.02	0.05	1.17	0:12
PD SJ010955.9-452800	23.28	0.14										
PD SJ010956.5-455900	21.53	0.02	20.48	0.02	19.32	0.02	18.94	0.02	18.38	0.02	0.253	0.32 0:02
PD SJ010957.3-453528	24.69	0.22	24.24	0.14	124.70	0.40	24.12	0.17	23.51	0.15	0.93	0:26
PD SJ010957.5-453457	22.07	0.03	20.96	0.02	19.81	0.02	19.38	0.02	18.78	0.02	0.242	0.32 0:02
PD SJ010957.6-462939	23.34	0.07	22.90	0.09	22.62	0.07			21.85	0.14		
PD SJ010958.2-461422	126.04	0.79	24.07	0.20	22.42	0.05			20.47	0.04		
PD SJ010958.6-453831	126.21	0.76	125.81	0.47	23.97	0.16	22.67	0.03	21.41	0.02	0.72	0:03
PD SJ010959.1-453340	22.29	0.04	20.77	0.02	19.31	0.02	18.68	0.02	18.10	0.02	0.28	0:01
PD SJ010959.2-454302	24.26	0.13	23.42	0.06	22.67	0.05	21.83	0.02	20.86	0.02	1.27	0:05
PD SJ011000.7-454727	24.50	0.14	23.93	0.08	24.25	0.22	23.44	0.07	22.34	0.04	0.94	0:10
PD SJ011001.4-455720	24.99	0.34	24.03	0.19	23.45	0.19	22.70	0.09	21.97	0.07	0.74	0:19
PD SJ011001.4-460819	22.15	0.02	20.61	0.02	19.72	0.02			19.13	0.02	3.056	
PD SJ011001.9-451842	21.17	0.02	20.21	0.02	19.48	0.02	19.04	0.02	18.64	0.02	0.32	0:06
PD SJ011002.0-453817	24.58	0.21	24.06	0.12	124.69	0.41	23.78	0.10	23.94	0.15	1.26	0:17
PD SJ011002.7-455945	25.29	0.24	24.44	0.14	24.15	0.18	24.34	0.14	24.19	0.16	0.24	0:04
PD SJ011002.9-461454	24.25	0.08	23.20	0.04	22.96	0.04			122.88	0.15		
PD SJ011004.5-461902	20.77	0.02	20.04	0.02	19.01	0.02			18.29	0.02		
PD SJ011004.7-454216	125.77	0.55	126.36	0.95	125.59	0.86	125.04	0.29			0.93	0:
PD SJ011004.9-450124	23.06	0.08	21.96	0.03	21.23	0.02	20.66	0.02	20.05	0.02	0.54	0:05
PD SJ011005.7-460127	22.38	0.02										
PD SJ011005.9-454035	> 25.30		125.34	0.37	24.46	0.31	23.96	0.11	23.80	0.13	0.36	0:08
PD SJ011006.0-462634	23.19	0.05	22.76	0.06	21.97	0.03			21.05	0.05		
PD SJ011006.2-452152	24.85	0.47	23.12	0.12	21.58	0.03	20.58	0.02	19.74	0.02	0.542	0.61 0:03
PD SJ011006.3-462111	22.76	0.03	22.30	0.03	21.99	0.03			21.55	0.08		
PD SJ011006.4-455735	24.18	0.09	23.67	0.08	23.02	0.07	22.40	0.03	21.38	0.02	0.93	0:04
PD SJ011006.8-450416	22.32	0.04	21.56	0.02	20.83	0.02	20.14	0.02	19.56	0.02	0.58	0:02
PD SJ011007.2-454727	24.31	0.11	23.82	0.07	23.02	0.07	22.54	0.03	22.17	0.03	0.50	0:06
PD SJ011007.5-462352	21.38	0.02	20.44	0.02	19.29	0.02			18.58	0.02		
PD SJ011007.6-451316	24.87	0.35	23.69	0.12	22.77	0.07	21.77	0.03	20.78	0.02	0.74	0:04
PD SJ011007.8-454748	24.63	0.19	24.55	0.18	125.05	0.55	24.51	0.23	23.92	0.18	0.95	0:24
PD SJ011008.2-450649	24.68	0.24	24.41	0.20	23.70	0.13	23.34	0.07	22.68	0.06	1.02	0:32
PD SJ011008.5-454022	126.21	0.89	125.81	0.58	125.38	0.73	24.51	0.19	23.07	0.09	0.71	0:12
PD SJ011008.5-451331	22.27	0.03	21.71	0.02	21.17	0.02	20.91	0.02	20.53	0.02	0.42	0:02
PD SJ011008.6-462908	20.82	0.02	20.16	0.02	19.09	0.02			18.50	0.02		
PD SJ011008.8-453022	23.28	0.08	22.17	0.03	20.91	0.02	20.17	0.02	19.51	0.02	0.357	0.49 0:03
PD SJ011009.2-453822	25.27	0.31	125.64	0.43	125.44	0.67	24.44	0.16	24.60	0.23	0.40	0:08
PD SJ011009.4-450829	23.78	0.13	23.43	0.10	22.70	0.07	22.16	0.04	21.17	0.03	0.93	0:04
PD SJ011009.6-460546	20.87	0.02	20.23	0.02	19.48	0.02			19.13	0.02		
PD SJ011009.7-453060	23.15	0.10	21.51	0.02	20.01	0.02	19.15	0.02	18.50	0.02	0.372	0.33 0:01
PD SJ011010.0-455355	24.26	0.20	23.27	0.10	22.36	0.07	21.60	0.02	20.90	0.02	0.66	0:07
PD SJ011010.3-453724	23.94	0.10	23.34	0.06	21.97	0.03	21.18	0.02	20.14	0.02	0.75	0:03
PD SJ011010.4-454405	21.65	0.02	20.62	0.02	19.44	0.02	19.04	0.02	18.49	0.02	0.33	0:02
PD SJ011010.8-460204	22.33	0.03										
PD SJ011010.8-450500	> 24.98		125.06	0.43	24.24	0.25	23.88	0.14	22.84	0.10	0.77	0:19
PD SJ011011.0-454117	23.94	0.11	23.48	0.07	22.78	0.07	22.33	0.03	21.33	0.02	0.93	0:03
PD SJ011011.5-451552	20.84	0.02	20.20	0.02	19.97	0.02	19.91	0.02	19.68	0.02	0.543	0.04 0:01

Table 6 | Continued

ID	U	B	V	R	I	K	$z_{\text{spec}}$	$z_{\text{phot}}$
PD SJ011011.5-450658	23.47	0.10	22.33	0.04	21.07	0.02	20.50	0.02
PD SJ011011.6-452742	18.50	0.02			17.28	0.02		0.32 0:03
PD SJ011011.7-455250	23.67	0.08	23.29	0.08	23.18	0.12	23.01	0.07
PD SJ011012.6-461706	24.06	0.09	23.23	0.07	21.83	0.02		1.18 0:23
PD SJ011012.9-453133	23.72	0.09	22.57	0.03	21.26	0.02	20.68	0.02
PD SJ011012.9-463056	22.81	0.04	22.45	0.05	22.02	0.03		0.31 0:02
PD SJ011013.3-453400	> 25.30		> 25.30		125.69	0.98	24.04	0.15
PD SJ011013.6-461915	23.53	0.12	22.77	0.08	21.10	0.02		20.22 0.04
PD SJ011013.7-454947	> 25.30		> 25.30		> 24.62		24.89	0.30
PD SJ011013.7-453936	24.55	0.28	23.03	0.07	21.61	0.04	20.56	0.02
PD SJ011014.0-452247	21.51	0.02	20.76	0.02	20.16	0.02	19.72	0.02
PD SJ011014.1-454420	24.09	0.12	23.35	0.07	22.62	0.07	21.85	0.02
PD SJ011015.4-461414	> 25.28		125.87	0.99	22.71	0.06		23.42 0.12
PD SJ011015.4-451338	125.46	0.60	23.48	0.10	22.05	0.04	21.06	0.02
PD SJ011015.4-455158	24.37	0.23	23.62	0.12	23.32	0.17	23.09	0.10
PD SJ011015.5-452918	23.88	0.15	23.44	0.10	22.69	0.10	21.69	0.03
PD SJ011015.5-455028	126.37	0.90	125.62	0.46	23.96	0.19	23.77	0.12
PD SJ011015.5-461106	> 25.28		> 24.82		125.01	0.62		21.74 0.14
PD SJ011015.5-453527	20.29	0.02	19.35	0.02	18.46	0.02	18.20	0.02
PD SJ011015.7-452515	24.44	0.41			21.80	0.07	21.59	0.06
PD SJ011016.1-455017	24.10	0.14	23.49	0.08	23.22	0.12	22.75	0.05
PD SJ011016.2-455822	> 25.10		125.43	0.43	124.36	0.25	24.50	0.19
PD SJ011016.2-454732	22.02	0.02	21.18	0.02	20.34	0.02	19.95	0.02
PD SJ011016.7-463259	22.85	0.08	21.18	0.03	19.73	0.02		18.30 0.02
PD SJ011017.0-453840	21.30	0.02	20.43	0.02	19.49	0.02	18.87	0.02
PD SJ011017.3-451000	125.34	0.62	> 24.63		125.31	0.78	24.39	0.29
PD SJ011017.4-453621	24.07	0.18	23.45	0.10	22.51	0.07	22.37	0.05
PD SJ011017.6-461760	23.29	0.08	22.86	0.09	22.32	0.06		21.82 0.04
PD SJ011017.8-453349	24.76	0.22	25.28	0.36	24.57	0.35	23.36	0.09
PD SJ011018.0-455559	17.98	0.02	16.51	0.02	15.69	0.02	15.35	0.00
PD SJ011018.0-451247	23.99	0.23	23.14	0.11	21.72	0.04	20.83	0.02
PD SJ011018.2-454904	21.36	0.03	20.49	0.02	19.65	0.02	19.40	0.02
PD SJ011018.2-463213	20.10	0.02	19.25	0.02	18.59	0.02		17.99 0.02
PD SJ011018.4-461204	24.86	0.23	24.52	0.25	23.55	0.11		21.70 0.09
PD SJ011019.2-453328	21.22	0.02	20.27	0.02	19.19	0.02	18.86	0.02
PD SJ011019.6-453858	20.40	0.02	19.53	0.02	18.62	0.02	18.36	0.02
PD SJ011019.6-455526	24.32	0.31	23.07	0.12	22.85	0.15	22.84	0.10
PD SJ011021.1-451144	23.63	0.11	22.90	0.06	22.54	0.06	21.91	0.03
PD SJ011021.2-454627	125.82	0.33	126.00	0.38	124.66	0.22	24.25	0.11
PD SJ011021.2-462518	21.58	0.02	20.27	0.02	18.80	0.02		23.34 0.07
PD SJ011021.2-455651	21.56	0.02	20.50	0.02	20.16	0.02	20.02	0.02
PD SJ011021.6-462559	19.94	0.02	19.28	0.02	18.45	0.02		18.02 0.02
PD SJ011022.5-453216	24.20	0.14	23.93	0.11	23.89	0.21	23.61	0.12
PD SJ011022.7-452037	126.21	0.99	124.96	0.39	24.50	0.26	24.62	0.25
PD SJ011023.4-450338	23.74	0.15	22.03	0.03	20.70	0.02	19.98	0.02
PD SJ011023.4-450206	> 24.98		24.60	0.38	> 24.63		23.75	0.18
PD SJ011023.9-452054	22.68	0.05	22.00	0.04	21.00	0.02	20.75	0.02
PD SJ011024.1-452459	23.85	0.12			23.68	0.20	24.06	0.29
PD SJ011024.4-451456	22.43	0.04	21.54	0.02	20.50	0.02	19.95	0.02

Table 6 | Continued

ID	U	B	V	R	I	K	$z_{\text{spec}}$	$z_{\text{phot}}$
PD SJ011024.6-460334	22.55	0.04	21.71	0.02	20.53	0.02	19.64	0.02
PD SJ011025.1-452355	21.84	0.03		19.74	0.02	19.38	0.02	
PD SJ011025.7-454431	126.39	0.74	125.77	0.45	125.63	0.74	24.65	0.17
PD SJ011026.8-454110	24.80	0.23	24.49	0.18	24.32	0.28	23.28	0.06
PD SJ011026.9-455247	24.52	0.24	24.10	0.21	24.02	0.32	23.90	0.20
PD SJ011027.2-453551	23.69	0.14	22.80	0.06	21.58	0.03	20.68	0.02
PD SJ011027.6-454702	24.06	0.09	23.58	0.06	23.42	0.10	23.46	0.07
PD SJ011027.7-460427	16.54	0.02	15.07	0.00				0.022
PD SJ011027.8-452255	21.39	0.03	19.86	0.02	18.38	0.02	17.93	0.02
PD SJ011027.8-454837	23.73	0.08	23.20	0.05	23.05	0.09	23.05	0.06
PD SJ011028.2-461228	23.93	0.14	23.57	0.15	23.20	0.12		21.69 0.14
PD SJ011028.3-453414	24.69	0.15	24.54	0.13	24.54	0.25	24.00	0.11
PD SJ011028.6-452439	22.56	0.06		20.07	0.02	20.01	0.02	
PD SJ011028.8-453747	126.00	0.42	125.40	0.25	> 24.62		25.00	0.18
PD SJ011029.5-461029	16.11	0.02	15.19	0.02				0.023
PD SJ011029.8-454858	22.07	0.02	21.29	0.02	20.46	0.02	19.85	0.02
PD SJ011030.2-453114	18.49	0.02	17.81	0.02	17.38	0.02		
PD SJ011030.9-460507	20.04	0.02	19.01	0.02	18.13	0.02		
PD SJ011030.9-463109	21.83	0.02	20.96	0.02	19.78	0.02		0.121
PD SJ011031.1-450028	125.38	0.56	24.32	0.23	125.39	0.77	23.66	0.14
PD SJ011031.4-450000	21.72	0.02	21.10	0.02	20.28	0.02	19.53	0.02
PD SJ011031.5-455123	23.75	0.08	23.17	0.05	22.86	0.07	22.34	0.03
PD SJ011032.1-454827	24.51	0.34	24.70	0.43	23.89	0.40	23.31	0.17
PD SJ011032.3-455745	23.72	0.10	22.93	0.06	22.80	0.08	22.52	0.04
PD SJ011032.4-454249	20.85	0.02	19.97	0.02	18.89	0.02	18.50	0.02
PD SJ011032.5-454004	22.49	0.04	21.61	0.02	20.53	0.02	20.00	0.02
PD SJ011032.5-454652	23.04	0.05	22.52	0.03	21.86	0.03	21.18	0.02
PD SJ011032.5-455404	21.46	0.02	20.01	0.02	18.60	0.02	18.09	0.02
PD SJ011033.3-454207	> 25.30		126.06	0.77	23.82	0.17	22.91	0.04
PD SJ011033.4-445958	23.39	0.11	22.77	0.07	21.92	0.04	21.11	0.02
PD SJ011033.4-452516	24.57	0.18		24.29	0.25	24.28	0.27	
PD SJ011033.6-460843	> 25.28		> 24.82		24.35	0.20		22.36 0.15
PD SJ011033.6-454021	22.08	0.04	21.06	0.02	19.92	0.02	19.15	0.02
PD SJ011033.8-455010	125.86	0.67	125.89	0.72	124.79	0.49	23.11	0.07
PD SJ011033.9-450756	19.80	0.02	18.47	0.02	17.42	0.02	17.07	0.02
PD SJ011033.9-460818	22.55	0.04	21.63	0.03	20.68	0.02		19.91 0.03
PD SJ011034.3-455122	126.43	0.73	125.44	0.30	125.10	0.42	24.07	0.12
PD SJ011035.1-452510	23.30	0.12		22.01	0.07	21.96	0.07	
PD SJ011035.8-445838	24.07	0.30	23.34	0.18	22.55	0.10	22.70	0.11
PD SJ011036.3-460657	> 25.28		> 24.82		24.46	0.23		21.96 0.12
PD SJ011036.4-453557	22.12	0.03	20.95	0.02	19.75	0.02	19.09	0.02
PD SJ011036.6-460013	23.57	0.08	23.01	0.07	22.45	0.06	21.88	0.03
PD SJ011037.0-461841	24.71	0.13	124.98	0.25	24.35	0.17		22.95 0.21
PD SJ011037.2-453259	> 25.30		> 25.30		125.37	0.73	24.05	0.16
PD SJ011037.2-451806	22.06	0.03	21.38	0.02	20.84	0.02	20.30	0.02
PD SJ011037.9-451131	23.04	0.07	21.82	0.03	20.87	0.02	20.45	0.02
PD SJ011038.0-451949	22.32	0.04	21.59	0.02	21.09	0.02	20.49	0.02
PD SJ011038.1-455830	125.44	0.45	23.93	0.14	23.39	0.13	22.72	0.05
PD SJ011038.2-453819	19.46	0.02	18.60	0.02	17.80	0.02	17.60	0.02

Table 6 | Continued

ID	U	B	V	R	I	K	$z_{\text{spec}}$	$z_{\text{phot}}$			
PD SJ011039.9-452333	23.31	0.09	22.20	0.05	21.54	0.03	21.11	0.02	20.65	0.02	0.10
PD SJ011040.7-455956	23.55	0.06	23.28	0.06	23.12	0.08	22.91	0.04	22.22	0.03	0.93
PD SJ011040.8-455119	23.62	0.07	23.21	0.05	23.11	0.08	22.66	0.04	21.93	0.03	0.94
PD SJ011040.8-454724	23.65	0.07	23.17	0.05	23.02	0.08	22.38	0.03	21.53	0.02	0.94
PD SJ011041.1-455421	> 25.10		24.86	0.49	124.64	0.60	23.16	0.10	22.05	0.05	0.65
PD SJ011042.0-454608	25.09	0.18	25.23	0.20	124.63	0.22	24.08	0.09	23.19	0.06	0.93
PD SJ011042.4-450706	125.59	0.70	24.16	0.20	23.21	0.10	23.28	0.09	23.21	0.12	0.22
PD SJ011042.4-450205	23.86	0.15	23.20	0.08	23.24	0.10	22.82	0.06	22.13	0.05	1.01
PD SJ011042.7-453119	> 25.30		24.29	0.18	23.75	0.21	24.04	0.21	23.66	0.20	
PD SJ011042.8-460022	> 25.30		25.06	0.49	23.70	0.21	23.26	0.09	21.78	0.04	0.72
PD SJ011043.0-452928	24.47	0.27	23.46	0.11	22.94	0.14	21.94	0.04	21.27	0.03	1.07
PD SJ011043.2-461050	20.56	0.02	19.64	0.02	18.43	0.02			17.69	0.02	0.229
PD SJ011043.7-453810	23.40	0.07	22.76	0.04	22.36	0.04	21.86	0.02	21.41	0.02	0.64
PD SJ011043.8-455104	24.27	0.10	24.07	0.09	23.43	0.09	23.23	0.05	22.47	0.04	0.94
PD SJ011044.3-455122	20.93	0.02	20.39	0.02	20.11	0.02	20.08	0.02	19.86	0.02	0.05
PD SJ011044.8-452227	23.46	0.11	21.83	0.03	20.52	0.02	19.67	0.02	19.08	0.02	0.38
PD SJ011045.1-450647	22.70	0.04	22.10	0.03	22.21	0.03	21.83	0.02	21.31	0.02	1.10
PD SJ011045.4-454626	> 25.30		25.26	0.48	24.28	0.36	23.46	0.13	22.56	0.08	0.72
PD SJ011045.8-463241	18.06	0.02	16.89	0.02	16.18	0.02			15.64	0.02	
PD SJ011046.1-451545	23.68	0.18	23.62	0.23	22.99	0.13	23.12	0.14	22.08	0.10	0.94
PD SJ011046.2-451434	24.59	0.18	24.24	0.15	23.84	0.13	23.79	0.11	23.72	0.15	0.23
PD SJ011046.5-461958	24.03	0.12	22.77	0.05	21.20	0.02			20.20	0.03	
PD SJ011046.6-454554	23.81	0.10	22.58	0.03	21.36	0.02	20.77	0.02	20.09	0.02	0.33
PD SJ011046.6-454554	23.81	0.10	22.58	0.03	21.36	0.02	20.77	0.02	20.09	0.02	0.33
PD SJ011046.6-451309	24.61	0.24	23.55	0.11	22.41	0.04	21.62	0.02	20.92	0.02	0.61
PD SJ011046.6-454141	18.62	0.02	17.58	0.02	16.88	0.02	16.64	0.00	16.22	0.00	0.120
PD SJ011046.7-454542	22.99	0.06	21.99	0.02	20.88	0.02	20.50	0.02	20.00	0.02	0.30
PD SJ011047.2-454739	24.44	0.16	23.79	0.09	22.70	0.06	21.85	0.02	21.12	0.02	0.67
PD SJ011047.3-453257	125.50	0.38	24.94	0.23	125.34	0.60	125.07	0.35	0.47	0.28	1.09
PD SJ011047.5-455410	24.66	0.15	24.25	0.12	23.98	0.14	23.79	0.08	22.91	0.05	0.94
PD SJ011047.5-445444	23.73	0.15	24.42	0.30	24.44	0.51	23.68	0.22	23.16	0.17	0.77
PD SJ011047.8-454638	22.43	0.03	21.49	0.02	20.42	0.02	19.94	0.02	19.43	0.02	0.263
PD SJ011048.0-460135	21.13	0.02									0.2
PD SJ011048.1-454441	23.48	0.09	22.78	0.05	22.07	0.05	21.59	0.02	20.63	0.02	0.93
PD SJ011048.2-462040	125.90	0.56	> 24.82		125.04	0.45			22.12	0.14	
PD SJ011048.3-454712	21.54	0.02	20.62	0.02	19.77	0.02	19.52	0.02	19.16	0.02	0.330
PD SJ011048.4-455908	125.77	0.46	125.49	0.44	24.47	0.26	24.13	0.13	23.62	0.11	0.61
PD SJ011049.1-462200	21.32	0.02	20.68	0.02	19.84	0.02			19.17	0.02	
PD SJ011049.3-450409	24.20	0.22	23.21	0.10	22.37	0.05	21.77	0.03	21.16	0.02	0.62
PD SJ011049.9-454819	126.06	0.83	> 25.30		125.17	0.73	24.68	0.32	23.09	0.12	20.56
PD SJ011050.1-455037	23.11	0.04	22.39	0.02	21.75	0.03	21.02	0.02	20.21	0.02	18.80
PD SJ011050.1-451708	125.13	0.46	24.54	0.33	24.41	0.31	23.74	0.16	22.68	0.10	0.94
PD SJ011050.5-462022	23.55	0.08	23.14	0.08	22.56	0.06			21.06	0.07	
PD SJ011051.3-461520	22.36	0.03	21.77	0.03	21.23	0.02			20.44	0.04	
PD SJ011051.6-460227	21.36	0.02	20.84	0.02	20.33	0.02			19.59	0.02	0.570
PD SJ011052.0-454340	22.01	0.02	21.22	0.02	20.34	0.02	19.93	0.02	19.45	0.02	18.27
PD SJ011052.2-453354	21.01	0.02	19.88	0.02	19.12	0.02	18.80	0.02	18.30	0.02	0.122
PD SJ011052.2-452125	24.55	0.32	23.03	0.09	21.45	0.02	20.80	0.02	20.21	0.02	0.23
PD SJ011053.1-460701	19.13	0.02	17.88	0.02	16.63	0.02					0.102

Table 6 | Continued

ID	U	B	V	R	I	K	$z_{\text{spec}}$	$z_{\text{phot}}$
PD SJ011053.5-454351	23.64	0.10	23.31	0.08	22.84	0.09	22.47	0.04
PD SJ011053.8-455211	23.48	0.10	23.05	0.07	23.07	0.14	22.11	0.04
PD SJ011053.9-461555	24.05	0.10	23.65	0.11	23.12	0.07		21.79 0.10
PD SJ011053.9-454339	> 25.30		25.18	0.46	23.76	0.23	21.98	0.03
PD SJ011054.1-455002	126.12	0.48	126.73	0.88	125.76	0.68	125.89	0.54
PD SJ011054.3-451653	22.45	0.05	21.20	0.02	19.96	0.02	19.54	0.02
PD SJ011054.7-455731	> 25.30		125.34	0.38	23.94	0.16	23.72	0.09
PD SJ011054.8-463156	23.76	0.07	23.80	0.14	22.98	0.06		21.69 0.08
PD SJ011054.9-453349	23.82	0.10	23.02	0.05	22.18	0.04	21.49	0.02
PD SJ011054.9-451152	20.28	0.02	18.98	0.02	17.96	0.02	17.55	0.02
PD SJ011055.1-450638	23.40	0.12	21.64	0.02	20.20	0.02	19.39	0.02
PD SJ011055.4-454625	24.46	0.17	23.85	0.10	24.06	0.22	23.91	0.13
PD SJ011055.5-460544	24.78	0.17	24.23	0.17	23.95	0.15		> 23.05
PD SJ011055.8-453920	17.68	0.02	16.63	0.02	16.20	0.02	16.02	0.00
PD SJ011056.3-452302	23.74	0.11	23.21	0.07	22.65	0.05	22.17	0.03
PD SJ011056.4-460944	24.32	0.15	22.58	0.05	21.08	0.02		
PD SJ011056.6-455302	23.62	0.15	23.48	0.17	23.40	0.24	22.43	0.07
PD SJ011056.8-460021	25.21	0.20	24.49	0.15	125.00	0.34	24.88	0.23
PD SJ011057.1-455211	> 25.30		23.99	0.20	22.23	0.08	21.03	0.02
PD SJ011057.2-454126	22.62	0.04	21.80	0.02	20.69	0.02	20.32	0.02
PD SJ011057.5-451735	22.39	0.07	21.28	0.03	20.10	0.02	19.47	0.02
PD SJ011057.5-451543	22.59	0.04	22.06	0.03	21.36	0.02	21.36	0.02
PD SJ011057.6-451430	> 24.98		23.32	0.09	22.02	0.03	21.41	0.02
PD SJ011057.7-461554	25.08	0.36	24.29	0.28	23.44	0.14		21.60 0.12
PD SJ011058.1-455736	125.74	0.48	24.43	0.18	23.94	0.17	22.91	0.04
PD SJ011058.8-455130	126.45	0.86	125.50	0.37	125.09	0.47	24.26	0.15
PD SJ011058.8-455130	126.45	0.86	125.50	0.37	125.09	0.47	24.26	0.15
PD SJ011058.9-453813	24.42	0.16	23.38	0.06	22.43	0.04	21.54	0.02
PD SJ011059.6-455444	126.52	0.50	126.16	0.42	125.33	0.29	125.50	0.23
PD SJ011100.0-452807	25.01	0.19						
PD SJ011100.3-455340	22.59	0.04	22.32	0.04	22.00	0.04	21.82	0.03
PD SJ011100.4-461910	24.21	0.16	23.35	0.11	22.19	0.04		20.77 0.05
PD SJ011100.7-453157	22.88	0.06	21.58	0.02	20.27	0.02	19.50	0.02
PD SJ011100.9-454940	> 25.30		126.82	0.75	126.09	0.72	126.23	0.56
PD SJ011101.2-454854	23.06	0.05	22.39	0.03	21.76	0.03	21.05	0.02
PD SJ011101.6-460019	24.45	0.17	22.68	0.05	21.50	0.03	20.54	0.02
PD SJ011101.7-454157	21.40	0.02	20.58	0.02	19.57	0.02	19.24	0.02
PD SJ011101.8-460122	24.33	0.13						
PD SJ011102.0-455319	24.32	0.13	23.77	0.10	23.39	0.11	22.96	0.05
PD SJ011102.1-454330	22.98	0.06	22.26	0.03	21.67	0.03	21.02	0.02
PD SJ011102.2-461824	23.99	0.18	23.02	0.11	22.20	0.06		21.51 0.14
PD SJ011102.5-450227	24.59	0.23	24.73	0.23	125.12	0.44	24.13	0.17
PD SJ011102.6-455135	> 25.30		> 25.30		124.66	0.31	23.32	0.06
PD SJ011102.6-454726	125.52	0.36	126.52	0.96	> 24.62		125.34	0.43
PD SJ011102.7-462743	24.04	0.17	22.73	0.09	21.15	0.02		19.45 0.02
PD SJ011103.0-455654	> 25.30		24.95	0.36	24.25	0.29	22.97	0.06
PD SJ011103.8-461556	23.64	0.10	22.91	0.09	21.67	0.03		20.37 0.04
PD SJ011103.8-455118	> 25.30		> 25.30		> 24.62		23.47	0.09
PD SJ011103.8-460305	25.04	0.37	23.49	0.13	22.10	0.04		20.44 0.04

Table 6 | Continued

ID	U	B	V	R	I	K	$z_{\text{spec}}$	$z_{\text{phot}}$
PD SJ011104.3-455532	126.22 0.56	> 25.30	> 24.62	24.52 0.14	23.26 0.06			
PD SJ011105.1-453007	> 25.30	> 25.30	125.22 0.67	24.30 0.21	24.00 0.20			
PD SJ011105.1-452040	> 24.98	> 24.92	126.14 0.61	125.18 0.24				
PD SJ011105.2-453850	24.13 0.13	23.32 0.06	22.15 0.04	21.26 0.02	20.43 0.02	18.63 0.02	0.538	0.70 0.00
PD SJ011106.1-454919	19.64 0.02	18.79 0.02	18.17 0.02	17.96 0.02	17.52 0.02	16.85 0.02	0.126	0.26 0.00
PD SJ011106.6-461048	23.29 0.08	22.35 0.05	21.23 0.02		20.08 0.03			
PD SJ011106.7-454536	22.38 0.02	21.76 0.02	21.17 0.02	20.72 0.02	20.33 0.02	19.41 0.04		0.48
PD SJ011107.0-460715	126.61 0.81	124.98 0.28	23.34 0.07		21.46 0.06			
PD SJ011107.5-455210	> 25.10	126.01 0.76	24.31 0.28	126.05 1.00				
PD SJ011107.7-461214	24.73 0.16	24.35 0.17	23.95 0.13		123.42 0.36			
PD SJ011107.7-453246	25.08 0.27	24.83 0.22	124.80 0.39	23.88 0.12	23.27 0.09			0.00
PD SJ011107.9-454026	126.46 0.82	24.39 0.12	125.28 0.50	24.77 0.19	24.55 0.20	122.92 0.79		0.24
PD SJ011108.0-453500	25.18 0.23	24.45 0.12	24.33 0.19	24.01 0.10	23.45 0.08			1.00
PD SJ011108.8-455129	23.88 0.15	23.24 0.09	23.26 0.17	22.58 0.07	21.76 0.04	19.32 0.07		1.15
PD SJ011108.8-453622	19.36 0.02	18.38 0.02	17.71 0.02	17.44 0.02	17.12 0.02			
PD SJ011109.4-460937	22.23 0.03	21.29 0.02	19.95 0.02				0.090	0.20
PD SJ011109.6-463232	23.20 0.06	22.44 0.05	21.46 0.02		20.56 0.04			
PD SJ011109.7-454820	126.52 0.61	125.90 0.40	125.02 0.32	24.79 0.18	23.64 0.09	20.87 0.11		1.14
PD SJ011109.9-460623	23.09 0.09	22.33 0.07	21.04 0.02		19.43 0.03			
PD SJ011110.1-461011	21.79 0.02	20.52 0.02	18.91 0.02		18.03 0.02			0.231
PD SJ011110.6-455555	> 25.30	> 25.30	23.71 0.17	23.78 0.12	23.03 0.08			
PD SJ011111.3-453501	> 25.30	> 25.30	> 24.62	23.83 0.15	22.70 0.08			
PD SJ011111.8-445635	21.39 0.02	21.76 0.02	21.82 0.02	21.95 0.03	21.54 0.02			1.00
PD SJ011112.3-450301	24.80 0.25	24.44 0.16	24.51 0.23	24.16 0.16	23.53 0.13			0.00
PD SJ011112.4-453013	125.51 0.33	24.52 0.14	23.90 0.14	23.27 0.06	22.22 0.03			0.00
PD SJ011112.7-455113	24.43 0.14	22.89 0.04	21.75 0.02	20.97 0.02	20.23 0.02	18.45 0.02	0.551	0.64 0.00
PD SJ011113.1-455123	> 25.30	125.64 0.58	> 24.62	24.14 0.18	23.30 0.11	20.78 0.18		
PD SJ011113.3-460922	21.84 0.05	21.10 0.04	20.50 0.03					
PD SJ011113.4-454011	23.45 0.05	22.89 0.03	22.73 0.05	22.33 0.02	21.41 0.02	19.60 0.04		1.03
PD SJ011113.4-455643	20.62 0.02	19.62 0.02	18.99 0.02	18.85 0.02	18.45 0.02			0.151 0.14
PD SJ011113.6-460060	20.06 0.02							
PD SJ011113.8-453602	24.78 0.39	24.34 0.26	> 24.32	23.39 0.14	22.57 0.09			1.00
PD SJ011113.9-455724	126.52 0.57	126.20 0.51	> 24.62	24.78 0.16	23.57 0.08			
PD SJ011113.9-460825	21.94 0.02	21.17 0.02	20.25 0.02		19.28 0.02			0.242
PD SJ011114.2-454250	125.60 0.34	24.57 0.13	23.73 0.11	23.19 0.04	22.45 0.03	19.80 0.04		1.03
PD SJ011114.2-455003	125.62 0.54	24.64 0.26	24.46 0.39	23.50 0.11	22.75 0.08	19.89 0.09		1.11
PD SJ011114.2-454724	125.70 0.53	25.16 0.37	125.50 0.91	24.19 0.19	22.50 0.06	20.44 0.13		0.71
PD SJ011114.3-460809	22.04 0.02	21.10 0.02	19.87 0.02		19.02 0.02			
PD SJ011114.4-451442	23.28 0.10	22.87 0.07	22.40 0.06	22.17 0.04	21.68 0.04			1.00
PD SJ011115.0-453214	22.67 0.04	21.07 0.02	19.64 0.02	19.00 0.02	18.40 0.02			0.301 0.30
PD SJ011115.2-454100	24.72 0.21	24.69 0.18	24.18 0.23	23.61 0.09	23.57 0.11	20.14 0.08		0.52
PD SJ011115.7-453204	21.93 0.02	21.08 0.02	20.07 0.02		19.17 0.02			0.370
PD SJ011115.8-454342	24.82 0.24	23.54 0.07	21.90 0.03	20.99 0.02	20.30 0.02	18.60 0.02	0.695	0.57 0.00
PD SJ011116.0-460938	21.27 0.02	20.84 0.02	20.36 0.02		20.25 0.02			1.058
PD SJ011116.3-453505	125.50 0.40	24.84 0.21	23.67 0.14	23.24 0.07	22.71 0.05			0.00
PD SJ011116.3-454107	21.72 0.02	21.22 0.02	20.92 0.02	20.45 0.02	20.00 0.02	19.43 0.06		0.59
PD SJ011116.4-453018	24.20 0.17	23.07 0.06	22.23 0.05	21.33 0.02	20.48 0.02			0.00
PD SJ011118.3-462855	125.92 0.56	> 24.82	23.57 0.11		21.46 0.07			
PD SJ011118.4-454629	21.12 0.02	20.19 0.02	19.21 0.02	18.90 0.02	18.43 0.02	17.45 0.02	0.234	0.31 0.00

Table 6 | Continued

ID	U	B	V	R	I	K	$z_{\text{spec}}$	$z_{\text{phot}}$
PD SJ011118.7-454338	24.19	0.09	23.59	0.04	23.30	0.06	22.84	0.03
PD SJ011118.8-451643	23.76	0.19	23.31	0.13	21.99	0.05	21.01	0.02
PD SJ011118.9-445903	21.99	0.03	20.86	0.02	19.84	0.02	19.40	0.02
PD SJ011119.1-455052	21.32	0.02	20.67	0.02	19.83	0.02	19.48	0.02
PD SJ011119.3-455556	15.50	0.02	14.19	0.00				0.022
PD SJ011119.6-451020	23.04	0.04	22.52	0.03	22.09	0.02	21.59	0.02
PD SJ011120.4-454543	25.27	0.21	24.84	0.15	24.38	0.17	24.59	0.14
PD SJ011120.6-461914	23.90	0.13	22.98	0.08	21.77	0.03		
PD SJ011121.0-454252	125.69	0.29	24.75	0.10	23.88	0.09	23.56	0.05
PD SJ011121.2-454430	21.71	0.02	21.06	0.02	20.26	0.02	19.99	0.02
PD SJ011122.0-455816	> 25.30		127.07	0.96	124.94	0.25	24.85	0.16
PD SJ011122.2-461014	23.78	0.13	22.81	0.07	21.83	0.04		
PD SJ011122.4-454701	22.98	0.05	22.16	0.03	21.41	0.02	20.75	0.02
PD SJ011122.6-450540	125.13	0.44	23.50	0.09	23.59	0.12	23.43	0.10
PD SJ011122.6-454000	22.66	0.04	22.23	0.02	21.73	0.02	21.31	0.02
PD SJ011122.9-452214	22.98	0.09	21.98	0.04	20.98	0.02	20.46	0.02
PD SJ011123.0-453032	25.11	0.23	24.36	0.10	24.43	0.21	24.68	0.20
PD SJ011123.2-454536	24.66	0.19	23.79	0.09	23.74	0.15	23.29	0.07
PD SJ011123.2-453517	125.69	0.39	125.43	0.28	> 24.62		24.39	0.14
PD SJ011123.8-455737	125.40	0.35	24.71	0.18	> 24.62		24.12	0.14
PD SJ011123.9-454343	21.81	0.02	21.27	0.02	20.52	0.02	20.20	0.02
PD SJ011124.2-450056	22.79	0.04	22.25	0.02	21.72	0.02	21.56	0.02
PD SJ011124.4-455404	125.72	0.29	25.24	0.17	124.99	0.25	23.82	0.06
PD SJ011125.1-452914	23.68	0.13	21.63	0.02	20.39	0.02		
PD SJ011125.3-451429	24.68	0.36	23.80	0.18	23.48	0.15	23.28	0.12
PD SJ011125.3-454725	> 25.30		126.06	0.62	124.83	0.35	24.45	0.17
PD SJ011125.7-453730	23.08	0.05	22.10	0.02	20.85	0.02	20.31	0.02
PD SJ011126.3-453815	19.94	0.02	18.95	0.02	18.04	0.02	17.68	0.02
PD SJ011126.4-453017	22.59	0.03	21.67	0.02	20.67	0.02	20.04	0.02
PD SJ011126.4-451605	> 24.98		125.32	0.54	125.10	0.50	24.25	0.21
PD SJ011126.6-462204	> 25.28		125.91	0.94	23.84	0.16		
PD SJ011126.8-455317	21.97	0.02	21.38	0.02	20.73	0.02	20.17	0.02
PD SJ011126.9-453416	20.80	0.02	19.91	0.02	19.15	0.02	18.88	0.02
PD SJ011127.2-454152	24.91	0.21	24.48	0.12	23.69	0.11	22.93	0.04
PD SJ011127.4-452106	21.24	0.02	20.52	0.02	19.82	0.02	19.58	0.02
PD SJ011127.5-454946	20.91	0.02	20.12	0.02	19.16	0.02	18.72	0.02
PD SJ011127.6-455832	25.00	0.21	24.86	0.18	125.13	0.42	24.07	0.11
PD SJ011127.6-454815	21.25	0.02	20.34	0.02	19.22	0.02	18.81	0.02
PD SJ011128.4-453827	> 25.30		125.36	0.23	24.25	0.16	23.18	0.04
PD SJ011128.5-455408	22.24	0.03	21.56	0.02	20.54	0.02	20.05	0.02
PD SJ011129.0-453054	> 25.30		125.98	0.69	124.88	0.47	24.62	0.27
PD SJ011129.6-455243	126.05	0.60	24.24	0.14	22.60	0.06	21.50	0.02
PD SJ011129.9-455029	25.30	0.32	24.52	0.17	125.67	0.85	24.17	0.16
PD SJ011129.9-455407	22.57	0.04	21.70	0.02	20.65	0.02	19.97	0.02
PD SJ011130.5-461635	24.63	0.18	23.62	0.09	23.29	0.08		
PD SJ011130.7-462118	24.18	0.15	23.65	0.14	22.81	0.07		
PD SJ011131.0-460842	24.57	0.19	23.95	0.15	23.35	0.10		
PD SJ011131.3-450011	16.59	0.02	15.41	0.02	14.88	0.00	14.72	0.00
PD SJ011131.4-454002	> 25.30		> 25.30		> 24.62		126.24	0.43

Table 6 | Continued

ID	U	B	V	R	I	K	$z_{\text{spec}}$	$z_{\text{phot}}$
PD SJ011131.4-455015	21.06	0.02	19.72	0.02	18.28	0.02	17.75	0.02
PD SJ011131.8-445119	21.66	0.03						
PD SJ011131.8-453814	21.91	0.02	21.39	0.02	21.00	0.02	20.60	0.02
PD SJ011132.2-455257	24.01	0.16	23.17	0.09	22.72	0.10	23.05	0.10
PD SJ011132.2-462421	24.62	0.21	23.79	0.15	22.95	0.08		
						21.31	0.08	
PD SJ011132.4-454938	> 25.30		> 25.30		> 24.62		125.53	0.43
PD SJ011132.5-451520	22.10	0.03	21.32	0.02	20.39	0.02	19.81	0.02
PD SJ011132.9-451757	20.21	0.02	19.07	0.02	18.23	0.02	17.95	0.02
PD SJ011133.0-450808	23.46	0.18	23.47	0.21	22.82	0.13	22.46	0.09
PD SJ011133.1-455951	> 25.30		24.40	0.20	23.80	0.21	22.13	0.03
PD SJ011133.2-453128	125.89	0.54	> 25.30		> 24.62		125.53	0.47
PD SJ011133.4-453222	20.01	0.02	19.62	0.02	19.64	0.02	19.57	0.02
PD SJ011133.7-450733	24.59	0.44	24.51	0.46	22.35	0.07	21.66	0.04
PD SJ011134.0-460526	125.34	0.40	23.01	0.07	21.50	0.02		
						19.91	0.02	
PD SJ011134.1-454609	22.29	0.04	21.34	0.02	20.29	0.02	19.65	0.02
PD SJ011134.7-455622	23.71	0.10	23.29	0.07	22.87	0.09	22.28	0.04
PD SJ011135.1-453245	18.66	0.02	17.42	0.02	16.58	0.02	16.26	0.02
PD SJ011135.5-455022	25.14	0.39	24.45	0.21	23.37	0.14	23.09	0.08
PD SJ011136.1-454249	23.99	0.10	22.58	0.03	21.35	0.02	20.80	0.02
PD SJ011136.1-453424	21.95	0.03	20.98	0.02	19.88	0.02	19.24	0.02
PD SJ011136.4-460505	23.96	0.12	22.89	0.07	21.43	0.02		
						19.94	0.02	
PD SJ011136.5-454155	24.78	0.25	23.71	0.08	23.82	0.17	23.52	0.10
PD SJ011136.9-445458	> 24.98		126.11	0.59	125.59	0.63	24.45	0.19
PD SJ011136.9-455805	19.88	0.02	18.82	0.02	18.20	0.02	17.95	0.02
PD SJ011137.0-462843	23.18	0.05	22.46	0.04	21.60	0.02		
						20.34	0.03	
PD SJ011137.0-454037	126.45	0.61	125.75	0.28	125.72	0.52	24.72	0.16
PD SJ011137.0-455252	20.29	0.02	19.47	0.02	18.74	0.02	18.53	0.02
PD SJ011137.6-454703	24.65	0.14	24.64	0.14	24.17	0.15	24.02	0.10
PD SJ011137.6-454525	24.53	0.14	23.79	0.07	23.08	0.06	22.71	0.03
PD SJ011138.1-453249	21.38	0.02	20.38	0.02	19.24	0.02	18.80	0.02
PD SJ011138.3-453357	22.87	0.04	22.20	0.02	21.61	0.02	20.96	0.02
PD SJ011138.6-453855	21.66	0.02	20.97	0.02	20.16	0.02	19.75	0.02
PD SJ011138.7-451018	> 24.98		124.99	0.36	124.72	0.32	24.20	0.19
PD SJ011139.4-451617	23.22	0.13	21.37	0.03	19.90	0.02	19.09	0.02
PD SJ011140.2-453907	22.54	0.06	20.86	0.02	19.39	0.02	18.53	0.02
PD SJ011140.3-454712	20.64	0.02	19.80	0.02	19.68	0.02	19.62	0.02
PD SJ011140.3-452252	24.91	0.34	23.66	0.11	21.96	0.03	20.96	0.02
PD SJ011141.1-455317	23.97	0.21	22.67	0.07	22.45	0.11	22.77	0.11
PD SJ011141.5-453535	> 25.30		> 25.30		> 24.62		24.13	0.14
PD SJ011141.9-451120	24.10	0.16	23.39	0.09	22.61	0.05	21.83	0.02
PD SJ011142.1-454020	23.60	0.08	23.14	0.05	23.14	0.09	22.53	0.04
PD SJ011142.2-454660	20.49	0.02	19.94	0.02	19.22	0.02	19.07	0.02
PD SJ011142.6-451831	18.33	0.02	17.81	0.02	17.85	0.02	17.82	0.02
PD SJ011142.8-462038	24.59	0.16	24.39	0.20	23.68	0.12		
						22.77	0.22	
PD SJ011143.9-455558	> 25.30		22.17	0.05	21.72	0.06	21.50	0.03
PD SJ011143.9-453702	25.28	0.32	24.41	0.15	23.88	0.16	22.80	0.05
PD SJ011144.2-462026	> 25.28		125.38	0.48	24.03	0.16		
						22.40	0.15	
PD SJ011144.7-455212	20.78	0.02	19.59	0.02	18.99	0.02	18.71	0.02
PD SJ011145.0-455650	22.81	0.04	22.28	0.03	21.85	0.04	21.36	0.02
						20.97	0.02	
							0.612	0.57

Table 6 | Continued

ID	U	B	V	R	I	K	$z_{\text{spec}}$	$z_{\text{phot}}$
PD SJ011145.6-454848	24.37 0.16	24.51 0.20	23.53 0.14	23.10 0.07	22.20 0.04	20.35 0.12		0.91 0
PD SJ011145.6-455818	> 25.30	24.75 0.23	24.42 0.32	24.32 0.21	23.36 0.12			1.19
PD SJ011145.6-451005	22.20 0.05	20.79 0.02	19.41 0.02	18.83 0.02	18.27 0.02			0.29
PD SJ011146.2-462110	125.36 0.45	24.64 0.36	23.40 0.13		21.19 0.07			
PD SJ011146.4-454019	23.06 0.07	21.27 0.02	19.74 0.02	18.88 0.02	18.22 0.02	16.87 0.02	0.370 0.33	0.33 0.01
PD SJ011146.9-445417	> 24.98	125.59 0.46	125.78 0.93	24.01 0.16	23.50 0.12			0.46
PD SJ011147.4-454028	24.07 0.13	22.34 0.03	20.88 0.02	20.02 0.02	19.33 0.02	17.91 0.02		0.35 0
PD SJ011147.6-451242	23.08 0.07	22.36 0.04	21.70 0.03	20.90 0.02	20.02 0.02			0.672 0.85 0
PD SJ011147.8-460830	23.43 0.08	22.45 0.05	21.07 0.02		19.81 0.02			
PD SJ011148.1-462140	20.60 0.02	19.82 0.02	18.84 0.02		18.24 0.02			
PD SJ011148.5-455757	23.55 0.06	22.96 0.03	22.66 0.05	22.27 0.02	21.53 0.02			1.28
PD SJ011148.7-455830	125.60 0.40	24.95 0.23	24.34 0.24	24.30 0.17	23.97 0.15			0.31
PD SJ011148.8-452438	23.77 0.17		22.07 0.07	21.67 0.05				0.649
PD SJ011149.4-461139	24.09 0.12	23.65 0.11	23.02 0.08		21.42 0.08			
PD SJ011149.5-455417	23.07 0.07	22.19 0.06	21.36 0.05		20.29 0.02			0.328
PD SJ011149.6-454207	23.57 0.06	22.75 0.03	21.60 0.02	21.11 0.02	20.58 0.02	18.88 0.03	0.743 0.39	0.03
PD SJ011150.2-453727	22.16 0.02	21.30 0.02	20.42 0.02	19.68 0.02	19.03 0.02			0.493 0.55 0
PD SJ011150.6-460014	23.30 0.05	22.93 0.04	22.71 0.07	22.00 0.02	21.15 0.02			0.94
PD SJ011151.2-450215	21.80 0.04	20.29 0.02	18.88 0.02	18.31 0.02	17.82 0.02			0.272 0.21 0
PD SJ011151.3-454322	21.62 0.02	20.83 0.02	20.00 0.02	19.47 0.02	18.98 0.02	17.78 0.02		0.48 0
PD SJ011151.5-455644	20.88 0.02	19.65 0.02	18.99 0.02	18.62 0.02	18.15 0.02			0.090 0.06 0
PD SJ011151.5-454444	23.01 0.04	22.42 0.02	21.94 0.03	21.45 0.02	21.04 0.02	20.32 0.05	0.496 0.55	0.03
PD SJ011151.6-454808	22.26 0.03	21.21 0.02	20.00 0.02	19.34 0.02	18.71 0.02	17.24 0.02		0.49 0
PD SJ011151.8-454102	125.46 0.26	25.27 0.20	24.45 0.18	23.80 0.07	22.71 0.04	19.99 0.05		1.00 0
PD SJ011152.4-453022	21.33 0.02	20.53 0.02	19.91 0.02	19.79 0.02	19.46 0.02			0.20
PD SJ011152.6-450828	> 24.98	> 24.92	126.00 0.87	24.26 0.17	23.13 0.10			
PD SJ011152.7-452336	> 24.98	23.37 0.15	125.09 0.79	24.51 0.45	> 24.54			
PD SJ011152.9-454024	21.82 0.02	20.77 0.02	19.75 0.02	19.34 0.02	18.77 0.02	17.52 0.02	0.228 0.36	0:02
PD SJ011152.9-455751	23.40 0.06	22.55 0.03	21.87 0.03	21.22 0.02	20.58 0.02			0.63
PD SJ011153.3-450157	23.39 0.08	22.88 0.05	23.08 0.08	22.47 0.04	22.04 0.04			0.84
PD SJ011153.3-450431	20.68 0.02	18.91 0.02	18.09 0.02	17.73 0.02				
PD SJ011153.5-455846	18.93 0.02	17.76 0.02	17.18 0.02	16.91 0.02	16.52 0.02			0.026 0.04 0
PD SJ011153.7-460727	20.03 0.02	18.89 0.02	17.74 0.02		16.98 0.02			0.134
PD SJ011154.2-453040	23.89 0.16	21.84 0.02	20.43 0.02	19.41 0.02	18.66 0.02			0.449 0.52 0
PD SJ011154.3-455409	20.87 0.02	19.77 0.02	18.89 0.02	18.49 0.02	17.94 0.02			0.136 0.29 0
PD SJ011154.4-450146	125.08 0.33	24.61 0.21	> 24.63	125.44 0.56	> 24.54			
PD SJ011154.6-454639	23.98 0.11	22.50 0.03	21.00 0.02	20.38 0.02	19.75 0.02	18.33 0.02	0.342 0.31	0:02
PD SJ011154.8-452733	21.88 0.03		19.47 0.02					
PD SJ011155.2-454214	20.40 0.02	19.55 0.02	18.61 0.02	18.29 0.02	17.79 0.02	16.83 0.02	0.229 0.35	0:02
PD SJ011155.6-453443	20.01 0.02	18.93 0.02	18.20 0.02	17.92 0.02	17.47 0.02			0.126 0.19 0
PD SJ011156.2-455008	23.31 0.06	22.54 0.03	21.98 0.04	21.40 0.02	20.62 0.02	19.41 0.05		0.76 0
PD SJ011156.3-455947	22.43 0.03	21.56 0.02						
PD SJ011156.3-452916	20.59 0.02	19.33 0.02	18.40 0.02		17.65 0.02			0.111
PD SJ011156.4-455834	18.75 0.02	17.43 0.02	16.46 0.02	16.06 0.00				0.089
PD SJ011156.5-460653	23.00 0.04	22.55 0.04	22.05 0.03		21.17 0.06			
PD SJ011156.6-460523	23.26 0.08	22.07 0.04	20.98 0.02		19.64 0.02			
PD SJ011156.7-453346	22.08 0.03	21.31 0.02	20.64 0.02	19.98 0.02	19.39 0.02			0.540 0.58 0
PD SJ011156.7-445450	19.70 0.02	19.14 0.02	18.41 0.02	18.15 0.02	18.23 0.02			1.053 0.27 0
PD SJ011156.7-454754	22.40 0.03	21.51 0.02	20.76 0.02	20.26 0.02	19.47 0.02	17.88 0.02	0.721 0.71	0:02

Table 6 | Continued

ID	U	B	V	R	I	K	$z_{\text{spec}}$	$z_{\text{phot}}$
PD SJ011156.9-461545	125.35	0.34	124.94	0.34	22.67	0.05	20.77	0.04
PD SJ011157.4-460456	24.23	0.16	23.09	0.09	21.93	0.04	20.61	0.05
PD SJ011158.0-452840	22.39	0.03						
PD SJ011158.3-454025	125.37	0.41	23.94	0.10	23.38	0.12	23.44	0.09
PD SJ011158.4-453419	126.46	0.94	24.64	0.17	24.13	0.20	22.89	0.05
PD SJ011158.7-450837	24.09	0.14	24.16	0.16	23.73	0.13	24.25	0.20
PD SJ011158.7-455210	21.49	0.02	20.60	0.02	20.48	0.02	20.25	0.02
PD SJ011159.1-450941	> 24.98		> 24.92		23.90	0.19	22.75	0.06
PD SJ011200.1-453356	125.51	0.37	24.62	0.15	23.70	0.13	22.61	0.04
PD SJ011200.3-455607	23.50	0.08	22.67	0.04	21.76	0.03	21.37	0.02
PD SJ011200.7-453941	125.59	0.36	125.53	0.31	125.45	0.56	24.64	0.20
PD SJ011201.6-451405	125.05	0.53	124.92	0.50	23.77	0.21	23.02	0.10
PD SJ011201.9-460203	125.49	0.28	24.66	0.16	23.72	0.08		
PD SJ011202.0-455429	24.41	0.14	25.03	0.23	125.20	0.51	23.91	0.12
PD SJ011202.4-460402	21.21	0.02	20.36	0.02	19.27	0.02		
PD SJ011202.6-453617	24.06	0.16	23.35	0.08	22.73	0.09	21.65	0.02
PD SJ011202.8-454302	19.56	0.02	18.55	0.02	17.98	0.02	17.78	0.02
PD SJ011203.7-461658	125.52	0.53	24.15	0.23	23.23	0.13		
PD SJ011203.8-455654	125.40	0.39	24.56	0.18	24.42	0.30	24.71	0.28
PD SJ011204.0-455848	> 25.30		25.14	0.30	23.76	0.16	22.56	0.04
PD SJ011204.0-455915	23.56	0.08	22.36	0.03	21.25	0.02	20.39	0.02
PD SJ011204.6-454448	21.03	0.02	20.06	0.02	18.93	0.02	18.55	0.02
PD SJ011205.3-452134	20.63	0.02	19.97	0.02	19.41	0.02	19.37	0.02
PD SJ011205.9-454622	24.83	0.24	24.33	0.16	23.56	0.14	23.57	0.10
PD SJ011206.0-453140	23.64	0.10	23.06	0.05	23.02	0.10	22.55	0.04
PD SJ011206.0-454601	24.78	0.27	125.23	0.40	24.07	0.24	23.79	0.13
PD SJ011206.5-455027	125.33	0.30	24.11	0.10	24.41	0.25	24.10	0.12
PD SJ011206.7-460910	21.07	0.02	20.44	0.02	20.41	0.02		
PD SJ011206.7-451721	23.28	0.12	22.44	0.06	21.54	0.03	20.86	0.02
PD SJ011206.7-452242	23.81	0.14	23.09	0.07	22.51	0.05	21.82	0.03
PD SJ011207.0-451625	> 24.98		> 24.92		124.81	0.27	24.07	0.13
PD SJ011207.2-453731	22.70	0.04	22.15	0.03	21.86	0.04	21.40	0.02
PD SJ011207.5-454616	> 25.30		126.28	0.66	> 24.62		125.08	0.27
PD SJ011208.0-454839	23.97	0.10	23.45	0.06	22.87	0.07	22.18	0.02
PD SJ011208.2-451143	20.38	0.02	19.39	0.02	18.87	0.02	18.70	0.02
PD SJ011208.3-450537	18.39	0.02	17.07	0.02	16.32	0.02	16.09	0.02
PD SJ011208.4-455402	24.46	0.14	24.39	0.12	23.27	0.08	22.59	0.03
PD SJ011208.8-455519	24.52	0.14	23.29	0.04	21.94	0.02	21.27	0.02
PD SJ011208.8-461840	24.65	0.15	23.64	0.09	23.18	0.07		
PD SJ011208.9-460510	23.97	0.13	23.65	0.14	22.96	0.09		
PD SJ011209.0-454324	24.25	0.11	23.76	0.06	23.66	0.11	23.01	0.04
PD SJ011210.2-454928	24.88	0.12	24.88	0.12	125.00	0.26	24.36	0.09
PD SJ011210.4-455607	21.26	0.02	20.57	0.02	20.14	0.02	20.05	0.02
PD SJ011210.7-463455	20.54	0.02			> 24.67			
PD SJ011210.9-454444	24.33	0.17	23.87	0.11	23.19	0.12	22.89	0.06
PD SJ011211.2-461504	125.53	0.35	24.68	0.22	23.95	0.14		
PD SJ011211.5-462902	19.02	0.02	17.97	0.02	17.39	0.02		
PD SJ011211.7-455818	24.47	0.17	23.15	0.05	21.90	0.03	20.97	0.02
PD SJ011212.1-454050	22.66	0.05	21.75	0.02	20.81	0.02	20.07	0.02

Table 6 | Continued

ID	U	B	V	R	I	K	$z_{\text{spec}}$	$z_{\text{phot}}$							
PD SJ011212.3-454758	125.78	0.48	25.09	0.27	23.93	0.17	22.85	0.04	21.84	0.02	19.98	0.08	0.69	0	
PD SJ011212.6-454435	23.29	0.09	22.60	0.05	21.62	0.04	21.01	0.02	20.45	0.02	18.44	0.03	0.85	0	
PD SJ011213.0-454018	24.37	0.14	23.47	0.05	22.80	0.06	22.01	0.02	21.42	0.02			0.64		
PD SJ011213.3-460322	21.49	0.02	20.84	0.02	19.89	0.02			19.26	0.02			0.364		
PD SJ011213.4-461006	25.24	0.23	24.77	0.23	24.30	0.18			123.53	0.38			0.328	0.62	0
PD SJ011214.5-450844	23.42	0.07	22.58	0.04	22.11	0.03	21.58	0.02	21.06	0.02			0.546		
PD SJ011215.0-452707	23.09	0.11			20.81	0.03	20.57	0.02							
PD SJ011215.2-454747	24.10	0.08	23.69	0.06	23.29	0.07	23.12	0.04	22.60	0.03			1.17		
PD SJ011215.2-462340	20.69	0.02	19.83	0.02	18.56	0.02			17.76	0.02			0.255		
PD SJ011215.3-460114	23.64	0.09													
PD SJ011215.4-453614	126.20	0.87	24.23	0.14	22.73	0.07	21.66	0.02	20.55	0.02			0.72		
PD SJ011215.6-461611	24.41	0.20	23.64	0.13	23.01	0.09			21.74	0.13					
PD SJ011215.8-451035	21.21	0.02	20.45	0.02	19.62	0.02	19.28	0.02	18.92	0.02			0.35		
PD SJ011215.9-461520	24.41	0.14	23.36	0.07	22.18	0.03			20.89	0.04					
PD SJ011215.9-452550	19.11	0.02			17.19	0.02	17.24	0.02					0.089		
PD SJ011216.1-454106	24.36	0.18	23.31	0.06	22.15	0.04	21.25	0.02	20.57	0.02			0.58		
PD SJ011216.5-454520	20.68	0.02	19.87	0.02	18.87	0.02	18.51	0.02	18.03	0.02			0.297	0.37	0
PD SJ011216.8-452653	23.07	0.07			21.02	0.02	20.78	0.02							
PD SJ011217.1-454306	24.11	0.11	23.38	0.05	22.46	0.04	21.70	0.02	20.85	0.02			0.77		
PD SJ011217.3-454816	125.33	0.37	24.44	0.17	24.42	0.31	23.84	0.12	23.40	0.10			1.20		
PD SJ011217.4-462932	> 25.28		125.50	0.76	24.35	0.31			21.24	0.08					
PD SJ011217.6-460920	24.77	0.21	24.16	0.19	23.55	0.13			22.60	0.24					
PD SJ011217.7-445837	24.09	0.24	22.75	0.10	21.87	0.05	20.91	0.02	19.68	0.02			0.703	0.73	0
PD SJ011217.9-455122	125.94	0.71	24.87	0.28	22.67	0.07	21.54	0.02	20.26	0.02			0.72		
PD SJ011218.2-460716	21.04	0.02	20.41	0.02	19.53	0.02			18.77	0.02			0.407		
PD SJ011218.3-453558	22.91	0.05	21.89	0.02	20.76	0.02	20.24	0.02	19.66	0.02			0.36		
PD SJ011218.5-455552	25.02	0.33	24.61	0.21	23.77	0.19	23.36	0.09	23.88	0.16			0.30		
PD SJ011218.5-452023	24.32	0.32	22.89	0.11	21.93	0.06	21.38	0.03	20.80	0.03			0.32		
PD SJ011218.8-452610	125.89	0.70			24.46	0.36	23.18	0.13							
PD SJ011218.9-453753	125.84	0.51	125.97	0.52	24.01	0.17	22.77	0.04	21.48	0.02			0.72		
PD SJ011219.1-461803	125.84	0.64	> 24.82		125.06	0.63			21.25	0.08					
PD SJ011219.3-451844	> 24.98				> 24.63		23.90	0.40	22.30	0.16					
PD SJ011219.7-455322	19.36	0.02	18.59	0.02	18.32	0.02	18.12	0.02	17.86	0.02			0.02		
PD SJ011220.0-454927	21.34	0.02	20.67	0.02	20.05	0.02	19.86	0.02	19.42	0.02			0.241	0.28	0
PD SJ011220.2-455154	23.32	0.08	22.44	0.04	21.55	0.03	20.66	0.02	20.02	0.02			0.60		
PD SJ011220.4-460759	23.94	0.09	23.56	0.10	22.64	0.05			21.75	0.10					
PD SJ011220.7-453948	22.16	0.02	21.41	0.02	20.75	0.02	20.04	0.02	19.47	0.02			0.465	0.57	0
PD SJ011220.8-452903	24.26	0.16	23.31	0.07	21.76	0.03									
PD SJ011221.5-455545	> 25.30		125.43	0.49	> 24.62		23.99	0.18	22.81	0.09					
PD SJ011221.6-452130	24.19	0.18			23.14	0.13	23.66	0.23							
PD SJ011222.4-461739	23.02	0.10	23.13	0.20	22.50	0.13			20.21	0.07			0.856		
PD SJ011222.6-461355	23.39	0.07	22.80	0.05	22.28	0.04			20.93	0.06					
PD SJ011222.9-453125	23.56	0.09	23.26	0.06	23.16	0.11	22.18	0.03	21.27	0.02			0.94		
PD SJ011223.4-460216	23.88	0.12	23.50	0.12	23.22	0.11			> 23.05						
PD SJ011223.6-460806	22.48	0.04	22.44	0.06	21.95	0.04			20.78	0.07					
PD SJ011224.3-450859	22.95	0.08			22.08	0.06	22.07	0.07							
PD SJ011224.4-445427	24.33	0.16													
PD SJ011224.6-455850	24.30	0.13	23.76	0.08	23.63	0.14	23.63	0.10	23.21	0.09			1.18		
PD SJ011224.8-455233	23.26	0.09	22.18	0.04	20.66	0.02	19.85	0.02	19.12	0.02			0.416	0.55	0

Table 6 | Continued

ID	U	B	V	R	I	K	$z_{\text{spec}}$	$z_{\text{phot}}$						
PD SJ011225.2-454700	20.25	0.02	19.55	0.02	18.88	0.02	18.73	0.02	18.30	0.02	0.236	0.26	0.02	
PD SJ011225.4-454351	24.94	0.26	23.82	0.09	23.56	0.13	23.00	0.06	22.49	0.05		1.16	0.12	
PD SJ011225.5-455937	125.74	0.53	24.90	0.24	125.54	0.84	24.08	0.16	23.80	0.16		0.66	0.27	
PD SJ011225.8-453857	24.09	0.23	22.76	0.06	21.83	0.05	21.18	0.02	20.56	0.02		0.58	0.04	
PD SJ011226.9-460910	23.50	0.10	23.19	0.11	22.47	0.07			21.65	0.14				
PD SJ011227.5-455851	23.68	0.07	23.06	0.04	22.59	0.05	22.11	0.02	21.17	0.02		0.94	0.05	
PD SJ011227.5-461718	24.81	0.20	24.15	0.18	22.94	0.07			21.34	0.07				
PD SJ011227.9-455041	24.48	0.17	23.31	0.06	22.30	0.04	21.47	0.02	20.55	0.02		0.74	0.04	
PD SJ011227.9-454450	> 25.30		> 25.30		> 24.62		> 25.03							
PD SJ011227.9-454308	24.21	0.16	23.71	0.09	23.48	0.15	23.06	0.07	22.55	0.06		1.19	0.77	
PD SJ011228.1-452637	> 24.98				24.18	0.30	23.45	0.18						
PD SJ011228.2-455843	> 25.30		> 25.30		> 24.62		23.82	0.18	22.26	0.07				
PD SJ011228.4-452155	24.63	0.40			22.81	0.15	22.05	0.08						
PD SJ011228.5-455637	> 25.30		24.83	0.24	24.52	0.34	23.93	0.15	23.91	0.17		0.29	0.07	
PD SJ011228.6-453612	22.05	0.03	20.84	0.02	19.57	0.02	19.05	0.02	18.45	0.02		0.32	0.01	
PD SJ011228.7-454960	23.21	0.06	22.17	0.03	21.06	0.02	20.53	0.02	19.86	0.02		0.298	0.42	0.03
PD SJ011228.8-454617	125.36	0.27	24.83	0.17	125.09	0.40	23.88	0.09	22.96	0.05		0.98	0.18	
PD SJ011228.9-455350	24.20	0.19	23.28	0.07	23.11	0.13	23.27	0.10	22.75	0.08		1.19	0.13	
PD SJ011229.1-452440	24.13	0.22			22.53	0.10	22.20	0.08						
PD SJ011229.2-453740	24.47	0.14	24.04	0.09	23.57	0.11	22.75	0.04	21.88	0.03		0.94	0.09	
PD SJ011229.4-455520	126.66	0.71	126.16	0.45	125.32	0.39	24.82	0.17	23.73	0.09		0.79	0.18	
PD SJ011229.7-454211	24.21	0.11	23.44	0.05	22.32	0.04	21.74	0.02	21.11	0.02		0.58	0.04	
PD SJ011229.8-445337	23.74	0.11										0.890		
PD SJ011230.4-454450	> 25.30		125.88	0.65	> 24.62		> 25.03							
PD SJ011230.4-453418	20.76	0.02	20.04	0.02	19.13	0.02	18.87	0.02	18.43	0.02		0.292	0.35	0.02
PD SJ011230.6-461223	23.77	0.10	23.20	0.09	23.12	0.10			22.27	0.21				
PD SJ011230.8-453710	125.58	0.80	> 25.30		23.65	0.26	22.14	0.05	21.40	0.04		1.04	0.09	
PD SJ011230.9-460027	25.05	0.28	23.79	0.12			23.30	0.09	22.81	0.09				
PD SJ011231.1-445809	> 24.98				22.94	0.14	22.56	0.12						
PD SJ011231.4-462755	24.56	0.21	124.97	0.44	23.25	0.11			21.37	0.09				
PD SJ011231.5-460226	24.98	0.24	24.44	0.21	22.53	0.04			20.56	0.03				
PD SJ011231.6-453737	24.25	0.14	23.48	0.07	22.66	0.06	21.89	0.02	21.19	0.02		0.70	0.05	
PD SJ011231.6-445836	18.24	0.02			16.73	0.02	16.84	0.02				0.082		
PD SJ011231.8-445609	23.05	0.07												
PD SJ011231.9-454523	24.76	0.18	24.61	0.17	23.75	0.14	23.64	0.09	23.31	0.09		0.42	0.09	
PD SJ011232.0-452946	23.88	0.08	23.23	0.04	22.81	0.06	22.65	0.04	22.17	0.03		1.21	0.08	
PD SJ011232.0-460556	21.19	0.02	20.59	0.02	20.27	0.02			20.21	0.02		2.240		
PD SJ011232.1-450834	22.94	0.08			20.66	0.02	20.43	0.02				0.378		
PD SJ011232.4-460625	24.69	0.21	24.22	0.20	23.70	0.15			22.43	0.22				
PD SJ011232.7-454759	22.72	0.04	22.09	0.02	21.62	0.03	21.14	0.02	20.43	0.02		1.14	0.05	
PD SJ011233.4-461137	21.65	0.02	20.99	0.02	20.29	0.02			19.98	0.02				
PD SJ011235.7-445506	23.76	0.10										0.540		
PD SJ011235.9-460208	21.13	0.02	20.78	0.02	20.34	0.02						0.611		
PD SJ011235.9-453934	22.50	0.03	22.04	0.02	21.74	0.03	21.37	0.02						
PD SJ011236.0-451804	22.61	0.07			20.62	0.02	20.65	0.02						
PD SJ011236.2-450517	23.56	0.15			22.72	0.13	22.93	0.18						
PD SJ011236.5-451842	20.95	0.02			18.06	0.02	17.90	0.02				0.235		
PD SJ011236.6-455620	21.80	0.02	21.14	0.02	20.38	0.02	20.06	0.02	19.67	0.02		0.374	0.39	0.02
PD SJ011236.6-455145	25.06	0.31	23.60	0.08	22.68	0.07	21.72	0.02	20.83	0.02		0.74	0.07	

Table 6 | Continued

ID	U	B	V	R	I	K	$z_{\text{spec}}$	$z_{\text{phot}}$
P D SJ011237.0-452240	> 24.98		22.30	0.13	21.74	0.09		
P D SJ011237.0-453854	21.29	0.02	20.46	0.02	19.58	0.02		0.138
P D SJ011237.2-460040	20.98	0.02	20.31	0.02				0.241
P D SJ011237.7-462914	24.80	0.23	23.82	0.13	23.46	0.12		
P D SJ011238.5-461853	20.64	0.02	19.85	0.02	19.01	0.02		0.185
P D SJ011238.5-462647	23.92	0.10	22.93	0.06	21.37	0.02		
P D SJ011240.3-453841	125.73	0.45	24.79	0.26	> 24.62	23.60	0.21	
P D SJ011240.5-451335	21.49	0.03			20.10	0.02		
P D SJ011240.7-460913	23.87	0.09	23.65	0.14	22.81	0.08		0.12
P D SJ011240.9-454955	24.89	0.36	24.43	0.29	> 24.62	23.19	0.12	0.28
P D SJ011241.0-460906	24.64	0.20	23.46	0.13	22.00	0.04		0.04
P D SJ011241.2-455226	25.03	0.54	24.03	0.29	23.17	0.24	21.20	0.03
P D SJ011241.2-452527	22.83	0.09			20.67	0.03		0.24 0.04
P D SJ011241.3-460323	20.93	0.02	20.55	0.02	19.81	0.02		0.313
P D SJ011241.4-453619	24.45	0.24	24.23	0.25	22.90	0.13	21.81	0.04
P D SJ011241.4-460358	24.21	0.16	23.21	0.14	21.92	0.05		0.698
P D SJ011241.8-453707	21.34	0.02	19.94	0.02	18.49	0.02	17.89	0.02
P D SJ011241.9-454720	24.77	0.28	24.39	0.23	23.08	0.15	22.34	0.05
P D SJ011243.1-463055	24.40	0.10	23.93	0.11	23.03	0.06		
P D SJ011243.4-460233	24.45	0.20	22.77	0.07	21.93	0.04		
P D SJ011243.7-453744	22.10	0.03	20.61	0.02	19.20	0.02		0.235
P D SJ011243.9-453544	24.61	0.15			23.91	0.19		
P D SJ011244.0-453548	24.21	0.13						
P D SJ011245.5-462856	24.14	0.11			23.90	0.02		
P D SJ011246.3-454048	22.24	0.04						
P D SJ011246.5-455853	21.21	0.02						0.360
P D SJ011247.4-461323	23.04	0.04			> 24.67			0.816
P D SJ011247.9-454450	21.43	0.03						0.239
P D SJ011248.0-461718	24.33	0.09			> 24.67			
P D SJ011248.1-455520	23.42	0.08						
P D SJ011249.2-455914	22.04	0.02						
P D SJ011250.1-454955	22.67	0.04						
P D SJ011250.6-455425	23.64	0.09						
P D SJ011251.1-461422	22.66	0.03			> 24.67			0.351
P D SJ011252.0-460037	19.48	0.02						0.132
P D SJ011252.7-454345	18.32	0.02						0.076
P D SJ011253.6-461815	24.28	0.14			> 24.67			
P D SJ011253.8-462720	23.61	0.07			> 24.67			
P D SJ011253.8-455209	22.73	0.03						0.613
P D SJ011253.9-462429	24.70	0.16			> 24.67			
P D SJ011254.7-453628	24.23	0.12						
P D SJ011254.7-455838	23.48	0.07						
P D SJ011255.0-453354	24.45	0.13						
P D SJ011255.3-462009	23.37	0.06			> 24.67			
P D SJ011255.5-454226	22.46	0.03						
P D SJ011255.6-455906	21.74	0.02						0.445
P D SJ011257.4-451746	19.69	0.02						0.144
P D SJ011259.3-453506	23.42	0.08						
P D SJ011259.6-455717	24.52	0.15						

Table 6 | Continued

ID	U	B	V	R	I	K	$z_{\text{spec}}$	$z_{\text{phot}}$
PD SJ011259.7-454717	23.58	0.05						
PD SJ011259.9-452419	23.90	0.13					0.369	
PD SJ011300.1-454121	20.09	0.02					0.096	
PD SJ011300.6-454910	24.69	0.16						
PD SJ011301.2-454128	23.90	0.10						
PD SJ011301.5-462436	23.38	0.05			> 24.67			
PD SJ011302.3-453418	22.53	0.06						
PD SJ011302.6-455034	24.41	0.14						
PD SJ011303.9-453009	18.57	0.02					0.086	
PD SJ011304.7-451905	20.99	0.02						
PD SJ011305.5-454903	24.20	0.12						
PD SJ011306.0-462603	18.93	0.02			> 24.67		0.066	
PD SJ011307.7-450603	20.36	0.02						
PD SJ011307.7-460532	23.51	0.10			> 24.67		0.368	
PD SJ011308.2-455750	22.88	0.08					0.447	
PD SJ011308.7-460537	20.28	0.02			> 24.67			
PD SJ011308.9-453034	23.27	0.05						
PD SJ011309.8-460933	23.46	0.07			> 24.67			
PD SJ011310.0-454037	19.86	0.02					0.096	
PD SJ011310.0-460556	22.19	0.02			> 24.67			
PD SJ011310.3-460951	24.15	0.14			> 24.67			
PD SJ011310.6-461015	23.07	0.06			> 24.67		0.272	
PD SJ011311.1-450145	18.50	0.02					0.082	
PD SJ011311.5-454302	23.37	0.09						
PD SJ011311.8-453611	25.07	0.16						
PD SJ011313.2-451634	22.09	0.04						
PD SJ011313.8-460157	19.80	0.02			> 24.67		0.134	
PD SJ011314.7-453701	22.75	0.08					0.368	
PD SJ011314.8-454051	23.06	0.08					0.985	
PD SJ011315.3-460560	22.21	0.07			> 24.67			
PD SJ011315.7-452201	23.06	0.13						
PD SJ011315.7-445919	19.85	0.02					0.235	
PD SJ011315.8-454632	23.63	0.06						
PD SJ011316.7-453654	24.72	0.14						
PD SJ011317.0-460207	24.39	0.17						
PD SJ011318.5-454715	21.30	0.02					0.332	
PD SJ011318.6-453400	19.91	0.02					0.230	
PD SJ011319.2-454531	23.09	0.07						
PD SJ011319.8-455447	23.45	0.12						
PD SJ011320.2-454556	24.14	0.16						
PD SJ011320.6-455524	21.27	0.07					0.419	
PD SJ011325.0-452254	17.74	0.02					0.030	
PD SJ011325.4-454218	20.92	0.03					0.121	
PD SJ011326.0-454910	19.63	0.02					0.253	
PD SJ011330.9-452121	23.41	0.18					0.327	
PD SJ011333.3-454731	20.63	0.02						
PD SJ011333.4-453841	21.44	0.06					0.276	
PD SJ011335.5-460048	21.15	0.08					0.234	
PD SJ011341.4-460114	19.67	0.04					0.132	

Table 6 | Continued

ID	U	B	V	R	I	K	$z_{\text{spec}}$	$z_{\text{phot}}$
PD SJ011345.4-452609	19.84	0.02					0.089	
PD SJ011348.6-455019	19.02	0.02					0.057	
PD SJ011349.2-454051	20.56	0.02					1.837	
PD SJ011354.1-452522	23.18	0.14						
PD SJ011355.1-452716	18.77	0.02					0.090	
PD SJ011356.7-453829	19.18	0.02					0.094	
PD SJ011357.3-453507	22.39	0.10						
PD SJ011400.4-454752	20.49	0.03						
PD SJ011403.7-455912	21.49	0.05					0.339	
PD SJ011405.3-452631	22.80	0.11						
PD SJ011406.0-450651	19.19	0.02					0.076	
PD SJ011406.0-454157	22.32	0.09					0.200	
PD SJ011407.6-451448	18.75	0.02					0.089	
PD SJ011407.6-451448	18.75	0.02					0.089	
PD SJ011411.1-452045	17.60	0.02					0.030	
PD SJ011413.9-455501	22.26	0.11					0.247	
PD SJ011414.7-451952	19.17	0.02					0.123	
PD SJ011414.8-455212	21.58	0.06						
PD SJ011415.2-454825	17.25	0.02					0.025	
PD SJ011416.5-452713	20.58	0.03					0.189	
PD SJ011421.2-450056	20.62	0.02						
PD SJ011425.3-450449	18.51	0.02					0.122	
PD SJ011426.5-455223	20.80	0.03					0.459	
PD SJ011431.9-451534	19.62	0.02						
PD SJ011432.7-453027	19.82	0.03						
PD SJ011432.9-452401	20.37	0.02					0.333	
PD SJ011442.4-452150	19.25	0.02					0.121	
PD SJ011442.5-452917	20.59	0.03					0.187	
PD SJ011442.8-452422	18.64	0.02					0.093	
PD SJ011453.8-455821	19.75	0.02					0.236	
PD SJ011454.1-454706	21.60	0.05					0.216	
PD SJ011457.6-445920	22.35	0.09						
PD SJ011457.8-450615	21.69	0.07					0.334	
PD SJ011459.9-445758	20.11	0.02					0.224	
PD SJ011503.5-454237	21.78	0.07					0.133	
PD SJ011506.8-455013	20.81	0.02						
PD SJ011508.3-455413	21.21	0.06					0.235	
PD SJ011522.1-455612	19.84	0.02					0.959	
PD SJ011534.2-454432	20.59	0.02					0.162	
PD SJ011537.9-450022	20.14	0.02						
PD SJ011539.6-455344	22.60	0.11					1.352	
PD SJ011540.1-454837	22.36	0.08						
PD SJ011544.8-455550	19.36	0.02					0.104	